MAPPING IRRIGATED AREAS IN ODISHA USING GOOGLE EARTH ENGINE (GEE)

A Thesis submitted to the Odisha University of Agriculture and Technology in Partial fulfilment of the requirements for the degree of Master of Technology in Agricultural Engineering (Soil and Water Conservation Engineering)

By

AISHWARYA VILAS DESAI

Adm. No. – 221421311

DEPARTMENT OF SOIL AND WATER CONSERVATION ENGINEERING

COLLEGE OF AGRICULTURALENGINEERING AND TECHNOLOGY

ODISHA UNIVERSITYOF AGRICULTURE AND TECHNOLOGY, BHUBANESWAR-751003

2024

ODISHA UNIVERSITY OF AGRICULTURE AND TECHNOLOGY
DEPARTMENT OF SOIL AND WATER CONSERVATION ENGINEERING
COLLEGE OF AGRICULTURAL ENGINEERING AND TECHNOLOGY
Bhubaneswar-751003, Odisha

Dr. (Mrs.) Prachi Pratyasha Jena
Assistant Professor

CERTIFICATE- I

This is to certify that the thesis entitled **"MAPPING IRRIGATED AREAS IN ODISHA USING GOOGLE EARTH ENGINE (GEE)"** Submitted in partial fulfillment of the requirements for the award of the degree of **Master of Technology (Agricultural Engineering) in Soil And Water Conservation Engineering** to the Odisha University of Agriculture and Technology, Bhubaneswar is a faithful record of bonafide and original research work carried out by **Miss Aishwarya Vilas Desai (Adm. No. 221421311)** under my supervision. No part of the thesis has been submitted for any other degree or diploma.

It is further certified that the assistance and help received by him from various sources during the course of the investigation has been duly acknowledged

PRJena

Bhubaneswar
Date: 20.08.2024

(Dr. (Mrs.) Prachi Pratyasha Jena)
Chairman
Advisory Committee

ODISHA UNIVERSITY OF AGRICULTURE AND TECHNOLOGY

DEPARTMENT OF SOIL AND WATER CONSERVATION ENGINEERING

COLLEGE OF AGRICULTURAL ENGINEERING AND TECHNOLOGY

Bhubaneswar-751003, Odisha

CERTIFICATE – II

This is to certify that the thesis entitled **"MAPPING IRRIGATED AREAS IN ODISHA USING GOOGLE EARTH ENGINE (GEE)"** submitted by **Miss Aishwarya Vilas Desai (Adm.No.221421311)** to the Odisha University of Agriculture and Technology, Bhubaneswar in partial fulfilment of the requirements for the degree of **Master of Technology (Agricultural Engineering) in Soil and Water Conservation Engineering** has been approved by the student advisory committee and the external examiner.

Advisory Committee

Chairman:

PRJena 4.9.2024

(Dr. (Mrs.) Prachi Pratyasha Jena)
Assistant Professor,
Dept. of SWCE, CAET, OUAT

Members:

4/9/2024

(Dr. Jagadish Chandra Paul)
Professor and Head,
Dept. of SWCE, CAET, OUAT

Ajit Kum Nayak

(Er. Ajit Kumar Nayak)
Scientist (SWCE), ICAR-IIWM
Bhubaneshwar

External Examiner:

Sonali Das 4.9.24

(Mrs) Sonali Das
Assistant Professor, Computer Sc.
Application, Dept. of MEE, CAET, OUAT

Suvan 4.9.24

Dr. Saswat Kumar Kar
Scientist, (SWCE)
ICAR-IISWC, RC, Koraput

ODISHA UNIVERSITY OF AGRICULTURE AND TECHNOLOGY
DEPARTMENT OF SOIL AND WATER CONSERVATION ENGINEERING
COLLEGE OF AGRICULTURAL ENGINEERING AND TECHNOLOGY
Bhubaneswar-751003, Odisha

PLAGIARISM CERTIFICATE

(For M. Tech Thesis)

This is to certify that the thesis entitled **"MAPPING IRRIGATED AREAS IN ODISHA USING GOOGLE EARTH ENGINE (GEE)"** submitted by **Miss Aishwarya Vilas Desai** bearing Admission No.**221421311, Department of Soil and Water Conservation Engineering, College of Agricultural Engineering and Technology, OUAT, Bhubaneswar** has been plagiarism checked (excluding cover pages) and has not crossed the limit as per the Anti-Plagiarism policy of OUAT.

Aishwarya Vilas Desai
Signature of the Student

P R Jena
20.8.2024
Signature of the Chairman
Advisory Committee

ACKNOWLEDGEMENT

I express my deep and sincere regards, the profound sense of gratitude and indebtedness to my guide as well as chairman of the Advisory Committee, Dr. Prachi Pratyasha Jena, Assistant Professor, Department of Soil and Water Conservation Engineering, CAET, OUAT, Bhubaneswar for untiring supervision, meticulous guidance and benevolent criticisms during the entire course of this investigation.

It is my high obligation to Dr. Sanjaya K. Dash, Dean, CAET, Odisha University of Agriculture and Technology, Bhubaneswar, for providing the necessary facilities in carrying out this piece of research work.

It is my pleasure to offer wholehearted and special thanks to Dr. Jagadish Chandra Paul, Professor and Head, Dept. of Soil and Water Conservation Engineering and Er. Ajit Kumar Nayak, Scientist at the ICAR-Indian Institute of Water Management, Bhubaneswar, for invaluable guidance and support throughout the course of this project. I am truly grateful for his mentorship and the confidence he instilled in me during this journey. I would also like to extend my heartfelt thanks to N M Jeepsa, SRF in IIWM Bhubaneswar for her constant support throughout this project. Her willingness to help, advice, and encouragement made a significant difference, and I am truly grateful for her presence at every step of this journey.

I would like to express my deepest gratitude to (Mrs) Sonali Das Professor, Computer Sc. Application, Dept. of MEE, CAET, OUAT for their guidance, and support throughout the period of the study and I place my special thanks to Dr. Bharat Chandra Sahoo, Professor, Retd. Professor, Dr. Ambika Prasad Sahu, Professor, Dr. Sanjay Kumar Raul, Associate Professor, Prabhat Chandra Pradhan, Asst. Professor Dept. of SWCE and for their valuable suggestion and help during my research work.

My sincere thanks to Ph.D. Scholars, batchmates and juniors for their support and encouragement rendered during the conduct of project work.

The graces of God have always blessed me and given me patience and power to overcome the difficulties which came in my accomplishment of this endeavour. I cannot dare to say thanks but only pray to bless me always.

Last, but not the least, I record my sincere thanks to my beloved and respected parents for their encouragement and blessings during my ups and down.

Above all my humble acknowledgment of the grace and blessing of the supreme power for enlightening my life and fulfilling this well-nurtured dream.

Aishwarya Vilas Desai

Place: Bhubaneswar **(Aishwarya Vilas Desai)**

Date: 20.08.2024 **Adm. No. 221421311**

CONTENTS

LIST OF FIGURES

LIST OF TABLES

SYMBOLS AND ABBREVIATIONS

Abbreviations	Expanded form
%	Percent
Th ha	Thousand Hecter
±	Plus minus
=	Equal to
GEE	Google Earth Engine
ML	Machine Learning
et al.	And all
Dept.	Department
Fig.	Figure
FAO	Food and Agriculture Organization
LULC	Land Use Land Cover
GAUL	Global Administrative Unit Layers
NDVI	Normalized Difference Vegetation Index
RF	Random Forest
SVM	Support Vector Machine
CART	Classification and Regression Tree
CAET	College of Agricultural Engineering and Technology
ICAR	Indian Council of Agricultural Research
MoA&FW	Ministry of Agriculture and Farmers Welfare
OUAT	Odisha University of Agriculture and Technology

ABSTRACT

Irrigation is vital for enhancing crop yield and stability by ensuring a consistent water supply, especially in areas with insufficient rainfall. Mapping irrigated areas is crucial for assessing water usage, optimizing irrigation practices, and improving agricultural productivity. Advanced technologies like remote sensing and machine learning provide accurate and detailed insights into irrigation patterns and practices. This study aims to accurately map and analyse irrigated areas in Odisha, India, from 2018 to 2023, using machine learning models within the Google Earth Engine (GEE) platform. Odisha, known for its diverse agricultural landscape, served as the study area. Sentinel-2 and Landsat-8 satellite data were utilized for Land Use Land Cover (LULC) classification and vegetation assessment, respectively. Classification and Regression Trees (CART), Random Forest (RF), Support Vector Machine (SVM), and Naive Bayes are among the machine learning models that were assessed. Of these, RF had the highest classification accuracy (94.60%). Various machine learning models, including Random Forest (RF), Support Vector Machine (SVM), Classification and Regression Trees (CART), and Naive Bayes, were evaluated, with RF achieving the highest classification accuracy of 94.60%. NDVI thresholds were applied to estimate district-wise irrigated areas during the Rabi season, with results validated against government-provided irrigation data. The study found a strong correlation between the estimated and observed values, with percentage errors ranging from 0.04% to 9.7% across districts. Spatio-temporal analysis revealed significant variations in cultivated and irrigated areas, with notable increases in both in 2020, followed by stabilization from 2021 to 2023. The findings demonstrate the effectiveness of GEE and RF models in monitoring and managing irrigated agriculture, offering valuable insights for agricultural planning and policy-making in Odisha.

Keywords: Google Earth Engine, Machine Learning, Random Forest Classifier, Irrigated Areas, NDVI, Land Use Land Cover, Spatiotemporal Analysis.

CHAPTER I

INTRODUCTION

Irrigation is crucial in agriculture as it ensures a reliable water supply, enhancing crop yields and supporting consistent food production, especially in regions with insufficient rainfall. It helps maintain soil moisture levels, improves crop growth, and can increase the diversity of crops grown, thereby boosting overall agricultural productivity and food security. Mapping irrigated areas is essential for managing water resources, ensuring food security, and understanding agricultural patterns. Globally, irrigated agriculture plays a vital role in food production, accounting for approximately 20% of the total cultivated land yet contributing to around 40% of the total food output (Rosegrant & Cline, 2003). In India, which holds one of the largest agricultural economies, irrigated land constitutes about 48.8 million hectares, making it the country with the largest irrigated area in the world. Odisha, a state with a predominantly agrarian economy, has about 6.4 million hectares of cultivable land, of which roughly 31% is irrigated (Mohapatra, 2016). Understanding the spatial distribution of these irrigated areas is essential for effective water management and agricultural planning. To achieve this, accurate mapping and monitoring of irrigated areas are essential.

Traditional methods of mapping irrigated lands, which often depend on ground surveys and limited remote sensing data, are filled with challenges. Because these procedures rely on human observation and interpretation, they are not only labour and time-intensive but also prone to a number of errors. The mapping of land use and cover has undergone a radical change in recent years due to the development of satellite imagery with high resolution and advances in remote sensing technologies. Remote sensing provides a brief view of the Earth's surface, enabling the capture of data over large geographic areas with high temporal frequency. This capability is particularly valuable for monitoring dynamic phenomena such as irrigation. By using the spectral and temporal characteristics of satellite imagery, it is possible to identify and determine irrigated areas with greater accuracy (Dong et al., 2016; Hemati et al., 2021; Mandal et al., 2017; Markert et al., 2018; Pham-Duc & Nguyen, 2022; Phiri et al., 2020). Satellites have revolutionized the process of mapping irrigated areas by providing high-resolution, time-series data that allows for continuous monitoring across large regions. Through remote sensing technologies, satellites capture critical data on vegetation

indices, moisture content, and land use, enabling the precise identification of irrigated fields. This data is invaluable for assessing irrigation patterns, detecting changes over time, and supporting sustainable agricultural practices (Alencar et al., 2020; Gumma et al., 2020; Tian et al., 2019; Waleed et al., 2022; Zohaib et al., 2019).

Google Earth Engine (GEE), a cloud-based geospatial processing platform, has emerged as a powerful tool for large-scale environmental monitoring and analysis (Tamiminia et al., 2020). GEE integrates a vast repository of satellite data with advanced computational capabilities, allowing researchers to perform complex geospatial analyses efficiently. The platform supports a wide range of datasets, including those from the Landsat and Sentinel satellite missions, which are particularly useful for agricultural monitoring, Land Use and Land Cover Mapping, Crop Health Assessment, Climate Change Analysis, Disaster Monitoring, Soil and Land Degradation, etc (Liu et al., 2018; Pandey et al., 2022; Taghizadeh-Mehrjardi et al., 2020; Wang et al., 2020).

The integration of machine learning algorithms with remote sensing data in GEE provides a powerful framework for mapping irrigated areas, Mapping of Vegetation Health, Mapping of Water Bodies, Mapping of Deforestation, Mapping of Flooded Areas, etc (Arpitha et al., 2023; Han et al., 2020; Liu et al., 2018; Pandey et al., 2022; Sazib et al., 2018. Machine learning models, such as Random Forest, Support Vector Machines, and Neural Networks, have demonstrated high accuracy in classifying land cover types based on spectral signatures. These models can be trained to distinguish irrigated lands from other land cover categories by learning from labelled training samples. Once trained, the models can be applied to classify large volumes of satellite imagery, enabling the generation of detailed irrigation maps.

Justification

The critical need for precise and timely information on water usage in agriculture, which is essential for sustainable water management and food security. Odisha, with its diverse agroecological zones, faces significant challenges in efficient irrigation management due to variable rainfall patterns and increasing water scarcity. GEE offers an advanced platform to monitor and analyse irrigated areas with high accuracy using satellite imagery and geospatial datasets. This enables better planning and allocation of water resources, improving agricultural productivity and resilience against climate change. Additionally, GEE's scalability and cloud-based processing

capabilities allow for comprehensive analysis over large areas and extended time periods. The insights gained can inform policy decisions, optimize irrigation practices, and contribute to the broader goals of environmental sustainability and economic development in Odisha.

This study aims to develop and implement a methodology for mapping irrigated areas in Odisha using machine learning models in Google Earth Engine. The study utilizes multi-temporal satellite imagery from Landsat and Sentinel-2 datasets, employing advanced machine learning techniques to achieve accurate classification of irrigated lands.

Objectives:

1) To evaluate four machine learning models in Google Earth Engine for mapping irrigated areas in Odisha

2) To estimate spatio-temporal distribution of irrigated areas in Odisha

REVIEW OF LITERATURE

CHAPTER II

REVIEW OF LITERATURE

The review of literature highlights application of Google Earth Engine (GEE) for precise irrigation mapping through satellite imagery and NDVI indices. Studies demonstrate GEE's scalability and cloud-based processing in overcoming data challenges, benefiting sustainable water management and agricultural productivity.

2.1 Application of Google Earth Engine in Agriculture

Amani *et al.* (2020) collected massive datasets for decades using Remote Sensing (RS). They explored GEE's by reviewing 450 journal articles published between 2010 and 2020. It found extensive use of Landsat and Sentinel datasets, widespread application of supervised machine learning algorithms like Random Forest, and diverse applications in land cover/use classification, hydrology, urban planning, natural disaster management, and climate analysis.

Pandey *et al.* (2022) focused on the 2020 floods in the Ganga-Brahmaputra basin, impacting regions in India (Bihar, West Bengal, Assam) and Bangladesh. Using Sentinel-1A Synthetic Aperture Radar data on the Google Earth Engine platform, the study estimated flood extents. Bangladesh experienced the largest flood area (25,889.1 km2), followed by Bihar, West Bengal, and Assam. The floods affected agricultural lands and settlements, impacting 23.68–28.47% and 5.66–9.15% of these areas, respectively. The study also assessed population impact, revealing 23.29 million people affected, with Bihar and Bangladesh facing the highest impacts due to their proximity to rivers and high population density. This spatial analysis provides valuable insights for decision-makers in flood risk reduction and management.

Velastegui-Montoya *et al.* (2023) highlighted GEE's potential in managing big satellite data and its multidisciplinary applications. The increase in geospatial data has driven the use of cloud-based tools like Google Earth Engine (GEE) for geoprocessing. A bibliometric analysis of GEE's scientific production from 2011 to 2022, using Elsevier's Scopus database, revealed 2800 documents from 125 countries, with China and the USA leading. Topics included satellites, sensors, remote sensing, machine learning, and land use.

Yang *et al.* (2022) reviewed literature to identify recent research integrating artificial intelligence (AI) methods with Google Earth Engine (GEE) for remote sensing

(RS) applications. They discussed major challenges in combining GEE and AI and highlighted priorities for future research. Additionally, they developed an interactive web application for dynamic review of the included publications.

2.2 Satellite based Irrigation Mapping

Phiri *et al.* (2020) shown Sentinel-2 is positive impact, especially in monitoring crops, forests, urban areas, and water resources. Its popularity is due to high spatial resolution (10 m), frequent updates (every 5 days), and versatile red-edge bands. Integrating Sentinel-2 with other data improves overall accuracy, and its free access policy encourages use, especially in developing countries. Studies indicate high accuracies (>80%) using machine-learning classifiers like SVM and RF. Despite challenges like mismatching with Landsat data and a lack of thermal bands, Sentinel-2 holds great promise for effective land cover monitoring.

Torbick *et al.* (2017) used Sentinel-1 C-band data which significantly improved large-scale rice agriculture assessment, especially in cloud-prone regions like South and Southeast Asia. Studies, such as those in Myanmar, have utilized Sentinel-1 and other satellite data with random forest algorithms to accurately map cropland and rice areas. This approach has demonstrated high accuracy (over 90%) and strong alignment with government statistics ($R^2 = 0.78$), highlighting the potential of Synthetic Aperture Radar (SAR) for effective agricultural monitoring.

Waleed *et al.* (2022) compared the effectiveness of three satellite datasets Sentinel-2, Landsat-8, and MODIS—for mapping rice crops in southern Punjab, Pakistan. The goal was to assess their accuracy in estimating rice-growing areas. Results showed that Sentinel-2 had the highest overall accuracy (96%), followed by Landsat-8 (91.7%) and MODIS (82.6%). The F1-Scores, which measure classification precision, were also highest for Sentinel-2. The estimated rice areas closely matched government statistics, with Sentinel-2 and MODIS having less than 20% mean percentage difference, while Landsat-8 had a 33% difference. Key findings suggest that higher spatial resolution improves mapping accuracy, Sentinel-2 is effective at distinguishing individual rice fields, and satellite data indicated a larger rice cultivation area than reported by the government.

Zohaib *et al.* (2019) introduced a new method to identify global irrigated areas by analysing satellite and reanalysis datasets. It relies on the observable effects of irrigation on three variables: soil moisture, land surface temperature, and surface albedo.

The method assumes that irrigation leaves distinct signatures in these variables that can be detected in near real-time through satellite observations. When compared to existing global irrigation maps, the new method shows reasonable agreement, overlapping with approximately 70% of the irrigated areas. This approach can enhance our understanding of water and energy balance on a large scale and minimize uncertainties in modelling irrigation impacts.

2.3 Mapping techniques in Google Earth Engine

Alencar *et al.* (2020) used 33 years (1985–2017) of Landsat imagery in Google Earth Engine to classify native Cerrado vegetation (NV) types and detect changes. Annual maps with up to 87% accuracy revealed a 0.5% annual decline in NV, primarily affecting forests and savannas, resulting in a loss of 24.7 million hectares. The findings highlight the challenge of mapping NV in this heterogeneous biome and indicate areas with higher rates of change.

Basukala *et al.* (2017) compared non-parametric machine learning algorithms (random forest and support vector machine) with a parametric algorithm (maximum likelihood) for agricultural land use mapping using Landsat 8 images. They assessed classifier performance using pixel-based and field-based approaches in Khorezm province and Republic of Karakalpakstan, Uzbekistan. The field-based non-parametric algorithms showed higher accuracy and kappa index compared to pixel-based and parametric methods. The study recommended field-based non-parametric algorithms for mapping irrigated croplands.

Gumma *et al.* (2019) aimed to create a precise cropland map for South Asia in 2015 using Landsat satellite data and machine learning on Google Earth Engine. With 900 million people facing food insecurity in the region, existing coarse-resolution maps lacked accuracy. Using 10 time-composited Landsat bands and machine learning algorithms, a 30-meter resolution cropland map was generated. The map showed a high accuracy of 89.9% in detecting cropland, with minimal errors. National and sub-national areas calculated from this map correlated well (80-96%) with official statistics. The full-resolution imagery is available for viewing, and the cropland products can be downloaded for further analysis.

Han *et al.* (2020) used Google Earth Engine to integrate climate, remote sensing, and soil data, predicting winter wheat yield 1-2 months before harvest with over 75% accuracy and less than 10% error. Support vector machine, Gaussian process

regression, and random forest were the top-performing models. The findings emphasize the effectiveness of multi-source data and machine learning for accurate crop yield prediction.

Latif *et al.* (2023) addressed water security and global food challenges, a high-resolution cropland extent product with 60 m precision is crucial. This study used eight Sentinel-2 instruments' data from 2018 to 2019 and pixel-based classification algorithms on the Google Earth Engine platform to create a detailed cropland map for Pakistan. Challenges included processing vast training and testing data across diverse locations, computational capacity, and handling large geographical datasets. The analysis used machine learning approaches (Random Forest, SVM, Naïve Bayes, and CART) and achieved an overall validation accuracy of 82%, with CART performing exceptionally well at 93%. The map revealed Pakistan's average cropland area and demonstrated the potential for measuring sub-national croplands. This research marks a conceptual shift in developing cropland maps using remote sensing multi-date techniques.

Nhamo *et al.* (2018) extracted agricultural fields in Venda and Gazankulu, Limpopo Province, South Africa, using Landsat 8 imagery from 2015 and a maximum likelihood supervised classifier. The NDVI applied during the dry season identified irrigated areas, achieving a 71% initial accuracy. Post-classification correction using UAV-acquired high-resolution aerial photographs improved accuracy to 95%.

Portmann *et al.* (2010) developed the global dataset MIRCA2000, which provided monthly irrigated and rainfed crop areas around the year 2000 at a spatial resolution of 5 arc min. It covered 26 crop classes, including major food crops and cotton, representing multi cropping systems and aligning with national and subnational statistics. The dataset revealed that 25% of global harvested areas were irrigated, with irrigated agriculture contributing to 33% of global crop production and 44% of total cereal production. Rice, wheat, and maize were the dominant crops, with rice having the largest irrigated harvested area.

Saad El Imanni *et al.* (2022) focused on accurately mapping crop types in the Tadla Irrigated Perimeter using Sentinel-1 and Sentinel-2 data and a Random Forest (RF) classifier with a Google Earth Engine (GEE) platform. The combination of these satellite data achieved an impressive 95.02% accuracy. The research also found that using monthly time series improves classification accuracy compared to single monthly images. Additionally, incorporating specific bands like red-edge and shortwave

infrared, along with vegetation indices and Sentinel-1 backscattering coefficients, enhanced overall accuracy. The best results were obtained with March images, achieving an accuracy higher than 80%. Overall, the study demonstrates the effectiveness of integrating various data sources and time series analysis for precise crop mapping in diverse agricultural landscapes.

Teluguntla *et al.* (2018) used Landsat-8 data and a random forest algorithm on Google Earth Engine to map cropland in Australia and China. Achieving high accuracy (97.6% for Australia, 94% for China), the method demonstrated its effectiveness in handling large data volumes and complex boundaries.

Thenkabail *et al.* (2009) aimed to compare satellite-based estimates of irrigated areas with official census data in India. Using data from 2000 at two resolutions (10-km and 500-m), the satellite results were compared with national statistics from the Ministry of Agriculture (DES) and the Ministry of Water Resources (MoWR). State-wise comparisons showed a good correlation, but satellite-derived estimates consistently exceeded official figures. The total area available for irrigation (TAAI) was 101 Mha (10-km) and 113 Mha (500-m), while irrigated areas (AIAs) were 132 Mha (10-km) and 146 Mha (500-m). In contrast, MoWR reported 83 Mha. Large variations in statistics were observed, even between different ministries, due to state reluctance and insufficient statistical analysis. Factors contributing to uncertainty included inadequate accounting for minor irrigation and groundwater, mapping challenges, difficulties in estimating irrigated area fractions, and satellite imagery resolution.

Tian *et al.* (2019) developed a method to composite multi-temporal NDVI from Landsat-7, -8, and Sentinel-2 images, using Google Earth Engine, for effective large-scale winter crop mapping. By identifying key NDVI periods and employing decision tree classification, the study achieved 96.22% accuracy and a kappa coefficient of 0.93. The method mapped 207,641 km² of winter crops in 2018, demonstrating its potential for rapid, accurate, large-scale applications.

Xiong *et al.* (2017) aimed to create a precise and accurate cropland map for Africa at a high spatial resolution (30-m or better) using Sentinel-2 and Landsat-8 data on Google Earth Engine. The map is crucial for food and water security analysis, enabling detailed assessments of irrigation methods, cropping intensities, crop types, fallows, productivity, and water usage. The study overcame challenges in mapping small-holder farms in Africa, a region with dynamic changes. The approach involved creating composite satellite images and using Random Forest and Support Vector

Machine algorithms for pixel-based classifications. The map achieved a weighted overall accuracy of 94%, estimating Africa's cropland area at 313 million hectares in 2015.

Zhang *et al.* (2022) used remote sensing and machine learning on Google Earth Engine to map irrigated farmlands at 500 m resolution. To overcome data limitations, they made provisional maps by combining statistics and satellite data, then refined them using an existing irrigation product and expanded dataset by incorporating irrigated croplands from three land use maps. Using locally adaptive random forest classifiers and various data sources, created detailed irrigation maps for each Chinese province on Google Earth Engine. Map excelled with 79.2% overall accuracy, outperforming others, and aligned well with statistical data at the province and prefecture levels (R^2 of 0.89 and 0.77, respectively). The map identified 87.04 million hectares of irrigated croplands in China in 2015. It revealed a strong correlation between irrigation and agricultural water use in Northwest, Northeast, and South China, but a weaker correlation in the North China Plain. This map aids national water resource management and decision-making for climate-resilient agriculture.

Zurqani *et al.* (2021) used satellite data and geospatial analysis to monitor irrigated and dryland agricultural areas in the South Atlantic Coastal Plain of South Carolina, USA. The goals were to track changes in irrigation over time, compare results with the United States Department of Agriculture (USDA) statistics, and provide valuable information for optimizing irrigation water use. The study uses high-resolution Sentinel-2 imagery on the Google Earth Engine platform, employing a random forest classification method. The maps created for three years (2016-2018) achieved overall accuracy ranging from 83.73% to 86.18%. The main irrigated crops are corn, cotton, soybeans, and peanuts, primarily concentrated in countries at the region's centre. This methodology can be applied to similar landscapes worldwide.

2.4 Irrigation studies using Remote Sensing

Angelakis *et al.* (2020) provided an overview of the evolution of irrigation practices from ancient times to the present, emphasizing techniques used by major civilizations such as the Egyptians, Minoans, Indus Valley, Chinese, Hellenic, Roman, Aztecs, Incas, Byzantines, Ottomans, and Arabs. It discussed how these ancient practices impacted modern water resource management and irrigated agriculture. The

study highlighted that adapting ancient irrigation techniques could address current agricultural water management challenges to enhance productivity and sustainability.

Meier *et al.* (2018) studied global irrigation mapping using multi-temporal NDVI SPOT-VGT data and agricultural suitability data from 1999 to 2012, revealing an 18% larger irrigated area than previous statistical-based approaches. The study found significant discrepancies in Asia, particularly in China and India, with more densely irrigated regions than previously estimated. Validation showed large divergences in existing datasets due to differences in spatial resolution, time periods, and input data.

Nhamo *et al.* (2020) improved agricultural water management and crop productivity by acquiring high-resolution spatial and temporal crop data at the field scale using Unmanned Aerial Vehicles (UAVs). UAVs with multispectral and thermal cameras monitored crops throughout the growing cycle, allowing timely detection and intervention for anomalies. This review synthesized the use of UAVs in smallholder agriculture in developing countries, highlighting their role in assessing crop health, evapotranspiration, water stress, and disaster risk reduction. The technology provided accurate statistics on irrigated areas and crop water requirements, improving water productivity and crop yield.

Nhemachena *et al.* (2020) studied climate variability and change in Capricorn District, South Africa, by assessing rainfall, temperature, and water stress trends from 1960 to 2015 using observed data and NDVI from 2000 to 2019. They found increasing drought frequency, rising temperatures, and heightened water stress, especially in rainfed smallholder farming areas. These findings underscore the need for localized adaptation strategies to address climate change risks.

Rayne *et al.* (2023) addressed the challenge of accurately mapping historical desertification in North Africa, focusing on the Skoura oasis in southern Morocco. Traditional maps often miss earlier desertification, but this study uses an open-source machine-learning approach with Google Earth Engine and the random forest algorithm. It classifies landcover categories, including a class for desertified fields, using Sentinel-2 and Sentinel-1 satellite data. The method achieved an accuracy of 74–76% for detecting desertification. Additionally, the study combines image interpretation and archaeological survey to map traditional irrigation systems supporting the oasis. This approach provides a more comprehensive understanding of historical desertification and traditional water systems in the region.

Riddell *et al.* (2019) reviewed KNP's investments in river management and current aquatic system status, highlighting case studies of diffuse pollution impacts on aquatic biotic processes. It compared these issues within a conservation management context to other KNP aquatic ecosystems where such impacts were not yet evident.

Arpitha *et al.* (2023) used machine learning methods on Google Earth Engine to classify Land Use and Land Cover (LULC) in Karnataka, India, from 2015 to 2021. Methods like Random Forest, Support Vector Machine, and Classification Regression Trees were applied using satellite images from Sentinel-2, Landsat-8, and MODIS. The major classes include Agricultural land, Built-up land, Forest land, Fallow land, wasteland, water bodies, and others. Agricultural land increased from 64.03% in 2015 to 67.81% in 2021, while water bodies grew from 5.25% to 6.3%. The largest category is agricultural land (64.03%), followed by forest land (19.65%). The rise in built-up land suggests rapid urban growth in major cities of the state. Overall, the study provides a reliable method for automated LULC classification in Karnataka.

Venkatappa *et al.* (2019) developed a simple yet effective method, called the Phenology-Based Threshold Classification (PBTC), to assess land use changes in Cambodia using Landsat satellite data. The method analysed the phenological behaviours of different vegetation types during leaf-shedding and leaf-flushing seasons, using the Enhanced Vegetation Index (EVI) and harmonic regression. By establishing threshold values for major land cover categories, the PBTC method produced a classified map with over 88% overall accuracy, especially effective in identifying forest cover with nearly 85% accuracy. The study highlights the utility of this method, particularly for assessing land use changes and carbon emissions in the context of global efforts like Reducing Emissions from Deforestation and forest Degradation (REDD+) scheme. The use of Google Earth Engine for accessing and processing large-scale remote sensing data was emphasized.

Thenkabail *et al.* (2007) established spectral matching techniques (SMTs) to determine land-use and land-cover (LULC) and irrigated area classes from historical time-series (HTS-LULC) AVHRR satellite data. It used target spectra from recent time series and ideal locations to map HTS-LULC from 1982 to 1985 and RTS-LULC from 1996 to 1999. The SMTs effectively identified and labelled HTS-LULC classes, with the spectral similarity value (SSV) method proving most accurate. The irrigated area in the Krishna River basin increased by 29.7% from 1982-1985 to 1996-1999, validating the SMT approach.

2.5 Machine Learning applications in Remote Sensing and Google Earth Engine

Magidi *et al.* (2021) used a non-parametric machine learning algorithm called random forest, along with Landsat and Sentinel satellite images, to classify irrigated areas in Mpumalanga Province, Africa. The process was automated on Google Earth Engine, with post-processing done using R-programming. The normalized difference vegetation index (NDVI) was employed to distinguish irrigated and rainfed areas during the 2018/19 and 2019/20 winter growing seasons. High NDVI values on cultivated land during the dry season indicated irrigation. The classification was done for 2020, with 2019 irrigated areas also classified to assess the impact of the Covid-19 pandemic on agriculture. The approach enhanced classification accuracy using ground-based training samples, very high-resolution images, fusion with existing datasets, and local knowledge, achieving an overall accuracy of 88%.

Ambika *et al.* (2016) developed a classification method for mapping irrigated areas in India from 2000 to 2015 using seasonal NDVI peaks in a hierarchical decision model. Calibrated for each agroecological region, the method produced accurate irrigated area maps that aligned with existing data and captured inter-annual variability, particularly during drought years. Despite the lack of traditional ground reference data, the results were consistent with published reports, suggesting the method's robustness. The study emphasized the potential of high-resolution NDVI data to further enhance accuracy, especially for small landholdings.

MATERIALS AND METHODS

CHAPTER III
MATERIALS AND METHODS

This chapter covers the study area, data utilized, and the methodology employed in the study. Detailed descriptions of the methodology for processing satellite imagery using Google Earth Engine (GEE) are provided. Additionally, the methodology for applying machine learning models to map irrigated areas is outlined. The analysis of temporal and spatial variations is also presented in this chapter.

3.1 Study Area

Odisha state is the study area, located between 17° 49' 25" to 22° 34' 30" N latitude and 81° 27' 35" to 87° 29' 30" E longitude. In the region, temperatures range from 10°C to 40°C during winters and summers, with occasional peaks up to 45°C. The annual rainfall varies from 1200 mm to 1800 mm within the study area. The soil of study area is predominantly red and laterite soil, with some areas of black soil. Odisha is known for its diverse agricultural practices, with major crops including rice, pulses, oilseeds, and cotton. The state's agricultural economy plays a significant role in its overall development, with agriculture employing a large percentage of the workforce. The State has 61.80 lakh hectares of total cultivated land, of which 29.14 lakh ha (47%) is high land, 17.55 lakh ha (28%) is medium land, and 15.11 lakh ha (25%) is low land. Irrigation makes up roughly 65% of the cultivated land. The study is covered with 30 districts. Fig. 3.1 and Table 3.1 shows the study area map and list of districts located in the study area respectively.

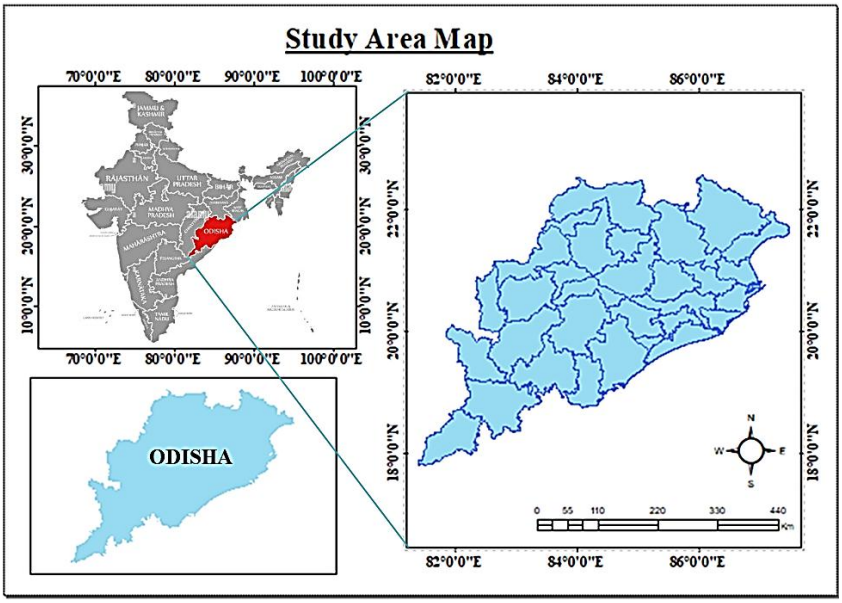

Fig 3.1. Location map of Odisha state

Table 3.1. List of districts lies in the Odisha

Sr.no	Districts	Sr.no	Districts
1	Angul	16	Kandhamal
2	Balasore	17	Kendrapada
3	Baragarh	18	Keonjhar
4	Bhadrak	19	Khordha
5	Bolangir	20	Koraput
6	Boudh	21	Malkangiri
7	Cuttack	22	Mayurbhanj
8	Deogarh	23	Nabarangpur
9	Dhenkanal	24	Nayagarh
10	Gajapati	25	Nuapada
11	Ganjam	26	Puri
12	Jagatsinghpur	27	Rayagada
13	Jajpur	28	Sambalpur
14	Jharsuguda	29	Subarnapur
15	Kalahandi	30	Sundargarh

3.2 Data Used

Various data used for the study are Sentinel-2 data, NDVI data, FAO data Irrigation data of year 2018 and ground truth data for LULC. Details of data sources are presented in Table 3.2.

Table 3.2 Detailed information of data used for this Study

SENTINEL-2 DATA	
Attribute	**Details**
Satellite	Sentinel-2 (Sentinel-2 Surface Reflectance (Level-2A))
Source in GEE	"COPERNICUS/S2_SR"
Used for	LULC map
Sensor	MultiSpectral Instrument (MSI)
Spatial Resolution	10 meters
Temporal Resolution	5 days
Spectral Bands for LULC	Blue (Band 2), Green (Band 3), Red (Band 4), NIR (Band 8), Red Edge 1 (Band 5), Red Edge 2 (Band 6), Red Edge 3 (Band 7), SWIR 1 (Band 11), SWIR 2 (Band 12)
Key Indices	NDVI, NDWI, NDBI
Cloud Masking	Sentinel-2 provides QA60 band and Scene Classification Layer (SCL) for cloud and cloud shadow masking.
Data Availability	Sentinel-2 data is available globally from 2015 onwards through platforms like Google Earth Engine (GEE).

LANDSAT-8 DATA	
Attribute	**Details**
Satellite	Landsat 8 (USGS Landsat 8 Level 2, Collection 2, Tier 1)
Source	LANDSAT/LC08/C02/T1_L2
Used for	NDVI threshold value
Sensor	Operational Land Imager (OLI)
Spatial Resolution	30 meters
Temporal Resolution	16 days (revisit time)
Spectral Bands for NDVI	Red (Band 4): 0.64 – 0.67 µm Near-Infrared (NIR, Band 5): 0.85 – 0.88 µm
NDVI Formula	NDVI=(NIR−Red)/(NIR+Red)
NDVI Range	-1 to +1 **-1 to 0:** Non-vegetated surfaces (e.g., water, built-up areas) **0 to +1:** Vegetated surfaces (higher values indicate denser vegetation)
Cloud Masking	Landsat 8 provides QA (Quality Assessment) bands for cloud masking, often used in NDVI calculations to filter out cloud and cloud-shadow pixels.
Data Availability	Landsat 8 data is available globally from 2013 onwards through platforms like Google Earth Engine (GEE).
FAO DATA	
Attribute	**Details**
Data	FAO GAUL (FAO Global Administrative Unit Layers 2015)
Source in GEE	"FAO/GAUL/2015/level2"
Used for	Extracting district boundaries for spatial analysis
Data Type	Administrative boundaries (polygons)
IRRIGATED AREA DATA	
Attribute	**Details**
Data	Irrigated area of year 2018
Source	Agricultural Statistics 2018
Publisher	Government of Odisha (Department of Agriculture & Farmers' Empowerment)
Used for	Validation of estimated irrigated areas
Geographical area	All districts of Odisha
Temporal coverage	Year 2018 (Rabi Season)
Validation Parameters	Total Area under irrigation and district-wise area under irrigation
Usage in study	Used to compare and validate the accuracy of irrigated area maps generated using Sentinel-2 and Landsat 8 data in GEE

3.3 Methodology

The methodology for this study involves evaluating machine learning models in Google Earth Engine (GEE) to map irrigated areas in Odisha and estimate their spatio-temporal distribution of irrigated areas for rabi season in year 2018-2023. This process includes the application of various algorithms to Sentinel-2 data to accurately classify LULC and using NDVI threshold value in Landat-8 imagery to accurately quantify irrigated regions. The analysis aims to capture changes over time and spatial variations, leveraging both estimated data and validation from agricultural statistics to ensure comprehensive and precise mapping.

Overview of methodology is shown in Fig. 3.2 and the steps of the methodology are given in subsequent sections.

3.3.1 Mapping of irrigated areas

District wise irrigated area map was develop using sentinel-2 and Landsat-8 data using machine learning models and NDVI threshold value.

3.3.1.1 Extraction of FAO and Sentinel -2 data

Accessing the FAO GAUL (Global Administrative Unit Layers) dataset, which provides detailed administrative boundaries, including districts and other administrative units. This dataset was imported into GEE to delineate the study area and accurately segment it by district for focused analysis. The reason for using FAO GAUL data was to ensure precise geographical boundaries that align with official administrative divisions, enabling a more accurate and region-specific analysis of land use, irrigation, and other environmental factors within the study area. This approach ensured that the spatial analysis conducted within GEE was both reliable and consistent with global standards.

Code: // Load FAO data for polygon boundary

```
var admin=table.filter(ee.Filter.eq("ADM1_NAME","Orissa"));
print (admin)
var dist=admin.filter(ee.Filter.eq("ADM2_NAME","Sambalpur"));
Map.addLayer(dist,{color:'yellow'}, 'dist');
```

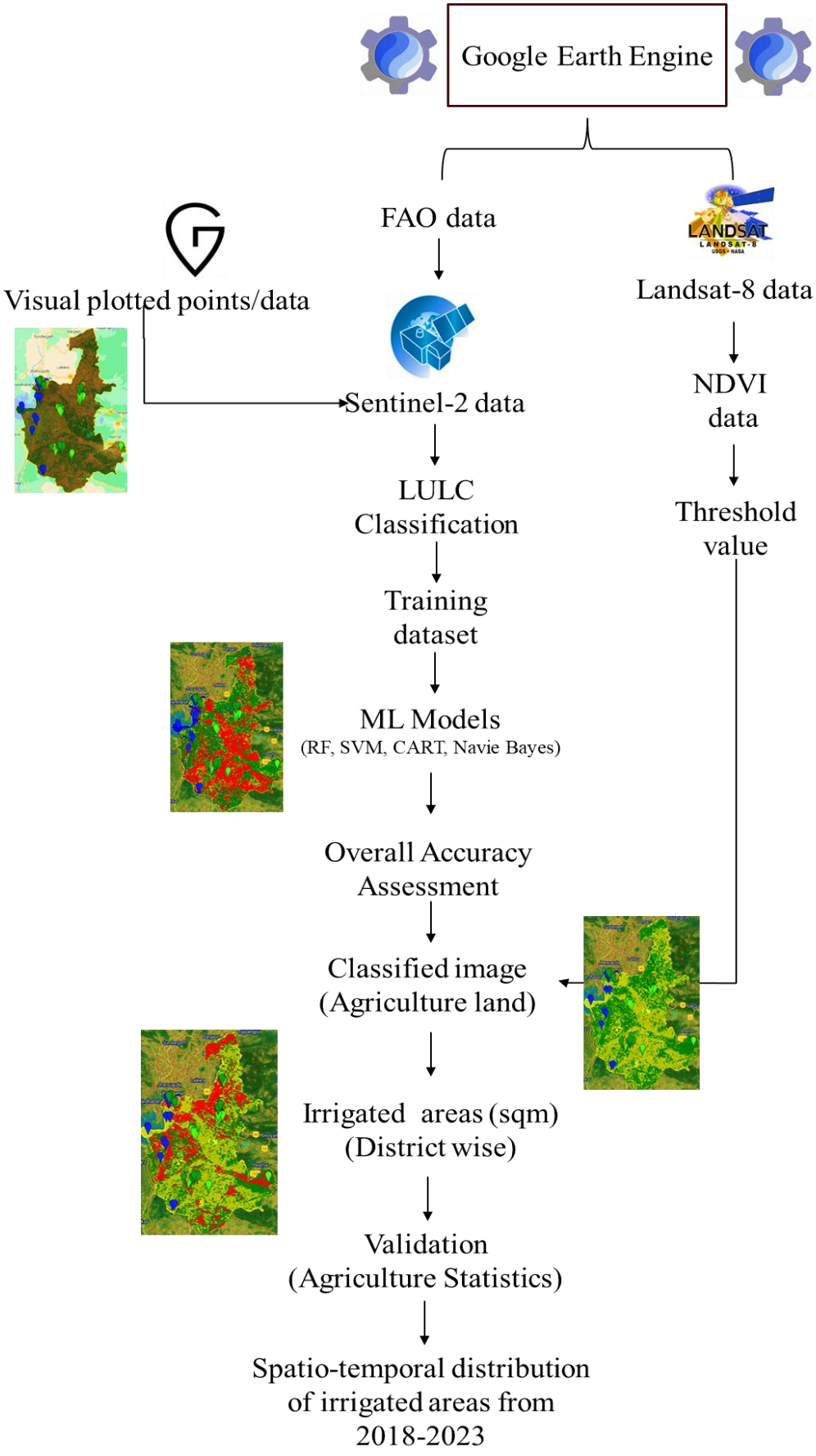

Fig. 3.2 Flow chart for mapping irrigated areas

Sentinel-2 surface reflectance data (COPERNICUS/S2_SR) was accessed through Google Earth Engine and pre-processed by applying cloud masks and atmospheric corrections to ensure data quality. Temporal composites were created to obtain cloud-free imagery. Training data for various LULC classes was collected by plotting visual datasets, and machine learning models, such as Random Forest, Support Vector Machine, CART and Navie Bayes were trained on these features.

Code: // Load all sentinel 2 images within polygon boundary

```
var s2 = ee.ImageCollection("COPERNICUS/S2_SR_HARMONIZED");
var image = s2.filter(ee.Filter.lt('CLOUDY_PIXEL_PERCENTAGE',30))
        .filterDate('2018-2-01','2018-05-31')
        .filter(ee.Filter.bounds(dist))
        .mean()
        .clip(dist);
var visualization = {min: 0.0,
                     max: 3000,
                     bands: ['B4', 'B3', 'B2'],};
Map.addLayer(image, visualization, 'RGB');
```

3.3.1.2 Identification of ground truth points for land use classification

Visual data points were plotted in GEE using Sentinel-2 data to classify land cover into four distinct categories: water, agriculture, forest, and built-up areas as shown in the Table 3.3 and Fig.3.3. A total of 390 points were carefully selected and distributed across these classes to ensure accurate identification and representation of each land cover type. These points served as training data for the machine learning models, helping to improve the precision and reliability of the classification process within the study area. By leveraging these points, the models were able to accurately differentiate between the various land cover types, leading to a more detailed and accurate mapping of the region.

Table. 3.3 List of Four distinct categories for LULC

Sr.no	Class	Land cover
1	Class 0	Water
2	Class 1	Agriculture land
3	Class 2	Forest
4	Class 3	Built-up

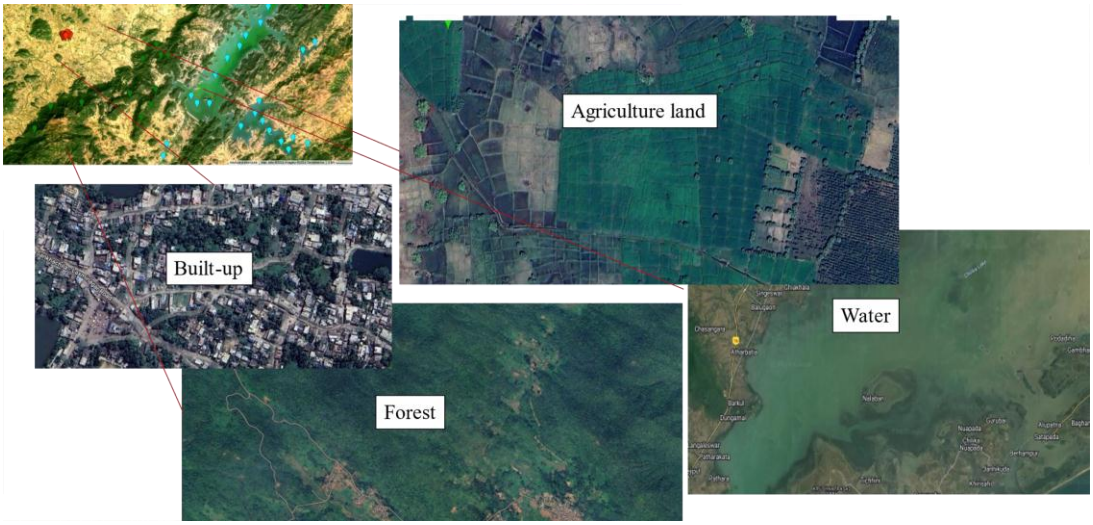

Fig. 3.3 Visually plotted ground control points in GEE

3.3.1.3 Training and testing of machine learning models for LULC classification

The next step involves using the plotted data points to train and test various machine learning models for LULC classification in GEE. The models used were Random Forest (RF), Support Vector Machine (SVM), Classification and Regression Trees (CART), and Naive Bayes. All 390 data points, representing the four land cover classes (water, agriculture, forest, and built-up areas) were merged across the study area in GEE. Relevant spectral bands from the Sentinel-2 imagery were selected to serve as input features for the ML models. The data points were then split into two sets: 80% for training the models and 20% for testing their performance. Each ML classifier was applied to the training set to develop a model capable of distinguishing between the different land cover types.

Code: // Merge all data

```
var sample = water.merge(agri).merge(vegetation).merge(builtup);
print (sample);
// Training and Testing data
var trainingDataset = training.randomColumn();
// 80% trainset
var trainset = trainingDataset.filter(ee.Filter.lt('random',0.8));
// 20% test set
var testSet = trainingDataset.filter(ee.Filter.gte('random',0.8))
```

Machine learning models, are widely used in land use and land cover (LULC) classification due to their ability to handle complex patterns in multi-dimensional

remote sensing data. These models improve classification accuracy by effectively distinguishing between different land cover types using spectral, spatial, and temporal features. Their adaptability and robustness make them essential tools in large-scale LULC mapping and monitoring. The models like Random Forest (RF), Support Vector Machine (SVM), Classification and Regression Trees (CART), and Naive Bayes were used. Further description of this machine learning models is given below one by one.

1. Random Forest (RF)

RF is an ensemble learning method that builds multiple decision trees during training. Each tree is trained on a random subset of the data, and the final classification is determined by averaging the predictions of all the trees. This helps reduce overfitting and improves accuracy. In GEE, RF is implemented by creating a forest of decision trees using selected spectral bands from the Sentinel-2 data. The model randomly selects subsets of training data and features, builds multiple trees, and aggregates their results to produce a final land cover classification.

Code: // Classification using Random Forest

```
var model = ee.Classifier.smileRandomForest(100).train({
 features:trainset ,
 classProperty: 'class',
 inputProperties:bands})
```

2. Support Vector Machine (SVM)

SVM is a supervised learning algorithm that works by finding the optimal hyperplane that separates different classes in the feature space. For LULC classification, SVM finds the boundary that best distinguishes between different land cover types based on the spectral values. In GEE, SVM is used by defining a kernel (e.g., linear, radial) and training the model to classify land cover classes by maximizing the margin between different LULC categories. The selected bands from Sentinel-2 are used as input features for the SVM model.

Code: // Classification using SVM

```
var model = ee.Classifier.libsvm(50).train({
features:trainset ,
classProperty: 'class',
inputProperties:bands});
```

3. Classification and Regression Trees (CART)

CART is a decision tree-based algorithm that splits the data into subsets based on the most significant feature at each node. The process continues until the subsets are sufficiently homogeneous, resulting in a tree where the leaves represent final classifications. In GEE, CART is implemented by building a tree where each node represents a decision based on the spectral values of the selected bands. The tree splits the data at each step to maximize the separation between different LULC classes, leading to a final classification based on the paths from the root to the leaves.

Code: // Classification using CART

```
var model = ee.Classifier.smileCart(50).train({
features:trainset ,
classProperty: 'class',
inputProperties:bands})
```

4. Naive Bayes

Naive Bayes is a probabilistic classifier based on Bayes' Theorem. It assumes that the features (e.g., spectral bands) are independent of each other given the class label. Despite this simplification, Naive Bayes often performs well in practice. In GEE, Naive Bayes calculates the probability of each land cover class based on the observed spectral values. It then assigns each pixel to the class with the highest posterior probability, using the selected bands as input features.

Code: // Classification using Navie Bayes

```
var model =ee.Classifier.smileNaiveBayes(50).train({
features:trainset ,
classProperty: 'class',
inputProperties:bands})
```

Each of these models in GEE uses the training data (80% of the total points) to learn the relationship between the spectral bands and the land cover classes. The models are then tested on the remaining 20% of the data to evaluate their accuracy in classifying LULC in the study area.

3.3.1.4 Overall accuracy assessment of machine learning models

Once the model is trained, it is tested using 20% testing dataset to predict the land cover classes. These predictions are compared against the true labels (the actual

land cover types) in the testing dataset. GEE generates a confusion matrix, which is a table that shows the number of correct and incorrect predictions made by the model. Each row of the matrix represents the instances in an actual class, while each column represents the instances in a predicted class for example as show in Table 3.4.

Table 3.4 Confusion matrix for Random Forest Model

Actual / Predicted	**Water**	**Agriculture**	**Forest**	**Built-up**	**Total**
Water	45	3	2	0	50
Agriculture	2	60	3	5	70
Forest	1	4	55	0	60
Built-up	0	3	2	45	50
Total	48	70	62	50	230

The overall accuracy is calculated by dividing the number of correctly classified instances (the sum of the diagonal elements of the confusion matrix) by the total number of instances in the testing dataset as shown in equation 1.

$$Overall\ Accuracy = \frac{Total\ Number\ of\ Pixels}{Number\ of\ Correctly\ Classified\ Pixels} \times 100 \quad \ldots\ldots\ldots\ldots\ 1$$

Other models were similarly assessed. The confusion matrix provided a detailed view of the classification performance across different land cover types, highlighting areas where the model performed well and where there might be misclassification. The results were used to determine the best-performing model for LULC classification in the study area.

The performance of each model was evaluated based on its overall accuracy and other metrics like producer's accuracy, user's accuracy and other metrics like Kappa coefficient, as calculated within GEE, to determine the best-performing ML model for LULC classification in the study area.

Producer's Accuracy

Producer's Accuracy indicates how well a particular class has been classified, and is calculated as shown in equation 2,

$$\text{Producer's Accuracy} = \frac{C_{ii}}{\sum_{j=1}^{n} C_{ij}} \times 100 \quad \ldots\ldots\ldots\ldots\ 2$$

Where,

C_{ii} is the number of correctly classified pixels for class

$\sum_{j=1}^{n} C_{ij}$ is the total number of actual pixels in class i (the sum of the row in the confusion matrix corresponding to class i).

User's Accuracy

User's Accuracy indicates the reliability of a class in the classification map and is calculated as shown in equation 3,

User's Accuracy = $\frac{C_{ii}}{\sum_{j=1}^{n} C_{ji}} \times 100$ 3

Where:

C_{ii} is the number of correctly classified pixels for class i.

$\sum_{j=1}^{n} C_{ji}$ is the total number of pixels classified as class i (the sum of the column in the confusion matrix corresponding to class i.

Kappa Coefficient

The Kappa Coefficient is a measure of agreement between observed and predicted classifications as shown in equation 4,

Kappa Coefficient $k = \frac{P_o - P_e}{1 - P_e}$ 4

Where,

Po is the observed agreement (i.e., overall accuracy).

Pe is the expected agreement by chance.

The Kappa Coefficient ranges from -1 to 1,

Where,

1 indicates perfect agreement.

0 indicates no agreement beyond chance.

Negative values indicate disagreement.

Code: // For Overall Accuracy Assessment

```
var classified_image = image.select(bands).classify(model)
Map.addLayer(classified_image,{min:0,max:3,
palette:['#0eeeff','#1ae312','#0f7b0b','#ff320a']},'LULC')
var confusion_matrix = ee.ConfusionMatrix(testSet.classify(model)
.errorMatrix({
        actual:'class',
```

```
                predicted:'classification'
              })
print(confusion_matrix)
print(confusion_matrix.accuracy())
print(confusion_matrix.kappa())
print(confusion_matrix.producersAccuracy())
print(confusion_matrix.consumersAccuracy())
```

3.3.1.5 Extracting agriculture land form classified image

After classifying the LULC in the study area using machine learning models, the agricultural land class was extracted for further analysis. This was achieved by isolating the agricultural class from the classified image and converting it from raster to vector format using the ee.Image.reduceToVectors() GEE. The resulting polygons, representing agricultural areas, were simplified to reduce complexity and remove small, isolated pixels. The final vector data was then validated against high-resolution imagery and existing agricultural boundaries to ensure accuracy before being exported for further analysis.

Code:
```
// Extracting Agriculture Boundary
var Agriculture_map = classified_image.eq(1).selfMask()
Map.addLayer(Agriculture_map , {min:0 , max:1 , palette:['green']},'Agriculture')
var Agri_boundary = Agriculture_map.reduceToVectors
                    ({
                    reducer: ee.Reducer.countEvery(),
                    geometry:ROI,
                    scale:300,
                    maxPixels:1e13
                    })
Map.addLayer(Agri_boundary)
```

3.3.1.6 Deriving irrigated land from Landsat-8 data using NDVI threshold value

The NDVI threshold value for distinguishing irrigated areas within agricultural land during the rabi season was derived using references from established research papers (Ambika et al., 2016; Magidi et al., 2021).

Landsat 8 imagery was utilized to calculate NDVI values, applying the following formula given in equation 5.

$$NDVI = \frac{(NIR-Red)}{(NIR+Red)} \quad \text{..... 5}$$

Threshold range 0.4 to 0.7 was identified in the literature were then applied to these NDVI values to accurately classify and differentiate irrigated areas from other agricultural lands. These threshold values helped in distinguishing between various vegetation conditions, ensuring precise identification of irrigated regions during the rabi season. The thresholds were validated against ground truth data and agricultural statistics to confirm their effectiveness and accuracy in the current study context.

Code: // Define the region of interest (ROI) and time period

```
var startDate = '2018-02-01';
var endDate = '2018-05-31';
// Filter Landsat-8 NDVI data
var LandsatNDVI = Landsat.filterBounds(Agri_boundary)
                          .filterDate(startDate, endDate)
                          .select('NDVI').map(function(img){
                          return img.multiply(0.0001)

.copyProperties(img,['system:time_start','system:time_end)'])
                          })
// Calculate the average NDVI for the agriculture class
var ndviMean = modisNDVI.mean().clip(Agri_boundary);
// Determine the threshold NDVI value
var classification = ee.Image(0)
                          .where(ndviMean.gt(0.4),1)
                          .where(ndviMean.lt(0.7), 2)
                          .rename('irrigated')
Map.addLayer(classification.clip(Agri_boundary),
{min:1,max:2,palette:['yellow']},'irrigated')
```

3.3.1.7 Estimating district wise irrigated area

The classified image of year 2018, which identified irrigated areas for rabi season, was combined with district boundary to overlay the irrigation classification into

the administrative boundaries of each district. This step involved merging the vector data of classified irrigated areas with district boundaries to facilitate spatial analysis. Using Google Earth Engine (GEE), the total area classified as irrigated was extracted for each district. The aggregated data provided the total irrigated area for each district. This calculation was carried out by applying the ee.Image.reduceRegions() function in GEE, which calculates the sum of pixel values within each district boundary. The resulting output was a dataset with the total irrigated area in hectares or square kilometres for each district.

Code: // District wise irrigated area in sqkm

```
var areaImage = classification.multiply(ee.Image.pixelArea())
var area = areaImage.reduceRegion({
        reducer: ee.Reducer.sum(),
        geometry:ROI.geometry(),
        scale: 300,
        maxPixels: 1e13 })
var AgrilAreaSQkm = ee.Number(area.get(classification)).divide(1e6)
print ("area of irrigation",AgrilAreaSQkm)
var areaImage = ee.Image.pixelArea().addBands(classification)
var areas = areaImage.reduceRegion({
        reducer: ee.Reducer.sum().group({
        groupField:1,
        groupName:'class'}),
        geometry:ROI.geometry() ,
        scale: 300,
        maxPixels: 1e13})
print(areas) //sqkm
```

3.3.1.8 Validation of estimated irrigated area

The irrigated area derived using the machine learning model based on remote sensing data and district-wise classifications, were compared with official agricultural statistics data provided by the Government of Odisha (Provide the reference). This involved overlaying the estimated irrigated areas on district boundary maps and extracting summary statistics for each district. These statistics were then compared against the reported figures from the government datasets. Discrepancies between the

remote sensing estimates and the statistical data were analysed to assess the accuracy of the remote sensing-derived estimates. Validation metrics percentage error was used to quantify the agreement between the estimated and observed data. This comparison ensured that the remote sensing estimates of irrigated areas were reliable and aligned with official agricultural records, thereby enhancing the credibility of the findings.

3.3.1.9 Temporal distribution of irrigated areas form 2018-2023

Validated classified images of irrigated areas for each year were prepared using the best performing machine learning model, ensuring accuracy through comparison with agricultural statistics. Using Google Earth Engine (GEE), the total irrigated area for each year was extracted and compiled into a time-series dataset. The changes in irrigated areas over time were assessed by calculating differences between consecutive years and analysing trends through statistical methods. Visualizations, including line graphs and maps, were created to depict the temporal variations effectively. The results were summarized to highlight variations and changes, providing a comprehensive view of how irrigation patterns have evolved over the specified period.

Sample code:

```
var admin=table.filter(ee.Filter.eq("ADM1_NAME","Orissa"));
//print (admin)
var dist=admin.filter(ee.Filter.eq("ADM2_NAME","Sambalpur"));
Map.addLayer(dist,{color:'yellow'}, 'dist');
var s2 = ee.ImageCollection("COPERNICUS/S2_SR_HARMONIZED");
var image = s2.filter(ee.Filter.lt('CLOUDY_PIXEL_PERCENTAGE',30))
          .filterDate('2022-2-01','2022-05-31')
          .filter(ee.Filter.bounds(dist))
          .mean()
          .clip(dist);
var visualization = {
  min: 0.0,
  max: 3000,
  bands: ['B4', 'B3', 'B2'],
};
Map.addLayer(image, visualization, 'RGB');

var sample = water.merge(agri).merge(builtup).merge(vegetation);
print (sample);

var bands = ['B1','B2','B3','B4','B5','B6','B7','B8','B9'];
//var bands = ['B1', 'B2', 'B3', 'B4', 'B5', 'B6', 'B7', 'B8', 'B9', 'B10', 'B11', 'QA_PIXEL',
'QA_RADSAT', 'SAA', 'SZA', 'VAA', 'VZA'];
var training = image.select(bands).sampleRegions({
  collection:sample,
  properties:['class'],
  scale: 60});
print(training);
```

```
var trainingDataset = training.randomColumn();
// 80% trainset
var trainset = trainingDataset.filter(ee.Filter.lt('random',0.8));
// 20% test set
var testSet = trainingDataset.filter(ee.Filter.gte('random',0.8));

//Random Forest classifier
var model = ee.Classifier.smileRandomForest(50).train({
  features:trainset ,
  classProperty: 'class',
  inputProperties:bands});

// //CART
var model = ee.Classifier.smileCart(50).train({
features:trainset ,
classProperty: 'class',
inputProperties:bands})

// // SVM
var model = ee.Classifier.libsvm(50).train({
features:trainset ,
classProperty: 'class',
inputProperties:bands});

// //NavieBayes
var model =ee.Classifier.smileNaiveBayes(50).train({
features:trainset ,
classProperty: 'class',
inputProperties:bands})
var classified_image = image.select(bands).classify(model);
```

```
Map.addLayer(classified_image,{min:0,max:3,
palette:['blue','green','yellow','red']},'classified');


var confusion_matrix = ee.ConfusionMatrix(trainset.classify(model)
.errorMatrix({
  actual:'class',
  predicted:'classification'}));
print(confusion_matrix);


print(confusion_matrix.accuracy());
print(confusion_matrix.kappa());
print(confusion_matrix.producersAccuracy());
print(confusion_matrix.consumersAccuracy());


// // //Chart
var chart = ui.Chart.image.byClass({
  image:ee.Image.pixelArea()
.multiply(1e-6)
.addBands(classified_image.rename('classification')),
  //image: classified_image,
  classBand:'classification',
  region:dist,
  reducer:ee.Reducer.sum(),
  scale:100,
  classLabels:['Water','Agriculture','Built up','Vegetation']}).setOptions({
    title:'LULC Area',
    vAxis:{title:'Area (sqkm)'},
    hAxis:{title:'Class'},
    bestEffort: true,
    colors:['blue','green','yellow','red']});
print(chart);
```

```
// // //single class map
var Agriculture_map = classified_image.eq(1).selfMask();
Map.addLayer(Agriculture_map , {min:0 , max:1 ,
palette:['grey','green']},'Agriculture');


Export.image.toDrive({
  image:Agriculture_map ,
  description: 'Agriculture',
  folder:'Progress',
  region: dist,
  scale: 60});

// // // Display the classified image
Map.addLayer(classified, {min: 0, max: 1, palette: ['green', 'red']}, 'Classified');

var Agri_boundary = Agriculture_map.reduceToVectors({
  reducer: ee.Reducer.countEvery(),
  geometry:dist,
  scale:100,
  maxPixels:1e13});
Map.addLayer(Agri_boundary);

var col = ee.FeatureCollection([Agri_boundary])
// //  Define the region of interest (ROI) and time period
var startDate = '2022-01-01';
var endDate = '2022-03-31';
```

```
// // // Filter LANDSAT NDVI data

var addNDVI = function(img){
  var ndvi = img.normalizedDifference(['B5','B4']).rename('NDVI');
  return img.addBands(ndvi);
};

Var Landsat8 =
ee.ImageCollection("LANDSAT/LC08/C02/T1_TOA").filterBounds(dist)
.filterMetadata('CLOUD_COVER', 'less_than', 1)
.map(addNDVI);
//print(Landsat8.size());
print(Landsat8.first());

//set start and end year
var startyear = 2016;
var endyear = 2024;

//make a date object
var startdate = ee.Date.fromYMD(startyear, 1, 1);
var enddate = ee.Date.fromYMD(endyear + 1, 1, 1);

//make a list with years
var years = ee.List.sequence(startyear, endyear);

//make a list with months
var months = ee.List.sequence(1, 12);

var annualndvi = ee.ImageCollection.fromImages(years.map(function (year)
{var annual = Landsat8
  .filter(ee.Filter.calendarRange(year, year, 'year'))
```

```
  .median();
  return annual
  .set('year', year)
  .set('system:time_start', ee.Date.fromYMD(year, 1, 1));
}));

//var annualprecip = addNDVI(annualprecip)
print(annualndvi);

var annualchart = ui.Chart.image.series({
  imageCollection:annualndvi.select(['NDVI']),
  region:dist,
  reducer:ee.Reducer.mean(),
  scale:30,
  xProperty:'system:time_start'}).setOptions({
    title:'Annual Time series chart',
    vAxis:{title:'value'},
    hAxis:{title:'year'}
  });
print(annualchart);

var monthlyndvi = ee.ImageCollection.fromImages(
  years.map(function (y) {
    return months.map(function(m){
      var w = Landsat8.filter(ee.Filter.calendarRange(y, y, 'year'))
            .filter(ee.Filter.calendarRange(m, m, 'month'))
            .median();
      return w.set('year', y)
      .set('month', m)
      .set('system:time_start', ee.Date.fromYMD(y, m, 1));
```

```
    });
  }).flatten()
  );
print(monthlyndvi);

var monthlychart = ui.Chart.image.series({
  imageCollection:monthlyndvi.select('NDVI'),
  region:dist,
  reducer:ee.Reducer.mean(),
  scale:30,
  xProperty:'system:time_start'}).setOptions({
    title:'Monthly Time series chart',
    vAxis:{title:'value'},
    hAxis:{title:'Month'}
  });
print(monthlychart);

// var L8NDVI = ee.ImageCollection("LANDSAT/LC08/C02/T1_TOA")
// .filterBounds(Agri_boundary)
//var L8NDVI = Landsat8.filterBounds(Agriculture_map.geometry())
var L8NDVI = Landsat8.filterBounds(Agri_boundary)
  .filterDate('2021-11-01','2022-05-31')
  .select('NDVI').map(function(img){
    return img.multiply(0.0001)
    .copyProperties(img,['system:time_start','system:time_end)']);
  });

// var a = ui.Chart.image.series(
// // {imageCollection:modisNDVI,
//   {imageCollection:L8NDVI,
```

```
//   region: dist,
//   reducer:ee.Reducer.mean(),
//   scale:60}
//   )
// print (a)

// // // Calculate the average NDVI for the agriculture class
// // //var agriculture = Agriculture_map;
// //var ndviMean = modisNDVI.mean().clip(Agri_boundary);
//var ndviMean = L8NDVI.mean().clip(Agriculture_map.geometry());
var ndviMean = L8NDVI.mean().clip(Agri_boundary);
// // // Determine the threshold NDVI value
var threshold = 0.4;

// // // Create a new image where pixels above the threshold are classified as irrigated and below as rainfed
var classified = ndviMean.gt(threshold).rename('irrigated');
Map.addLayer(classified, {palette:['red']},'ndvi');

// var classification = ee.Image(0)
// .where(ndviMean.gt(0.4),1)
// .where(ndviMean.lt(0.7), 2)
// //Map.addLayer(classification
.clip(Agri_boundary),
{min:1,max:2,palette:['green','red']},'classified ndvi')
// Map.addLayer(classification.
clip(Agriculture_map),
{min: 1,max:2,palette:['green']},'classified ndvi')

Export.table.toDrive({
collection:Agri_boundary ,
```

```
description:'Agriboundy',
folder:'GEE',
fileFormat:'SHP'});

Export.image.toDrive({
  image:ndviMean,
  description:'Argi_ndvi',
  folder:'GEE',
  region:dist,
  scale:30,
  maxPixels:1e13});

// //var areaImage = Agriculture_map.multiply(ee.Image.pixelArea())
// var areaImage = classified.multiply(ee.Image.pixelArea())

// var area = areaImage.reduceRegion({
//   reducer: ee.Reducer.sum(),
//   geometry:dist.geometry(),
//   scale: 100,
//   maxPixels: 1e13 })

// //var AgrilAreaSQkm = ee.Number(area.get('classified')).divide(1e6)
// var AgrilAreaSQkm = ee.Number(area.get('irrigated')).divide(1e6)
// print("area of irrigation",AgrilAreaSQkm)

// //var areaImage = ee.Image.pixelArea().addBands(classified_image)
// var areaImage = ee.Image.pixelArea().addBands(classified)

// var areas = areaImage.reduceRegion({
//   reducer: ee.Reducer.sum().group({
```

```
//     groupField:1,
//     groupName:'class'}),
//     geometry:dist.geometry() ,
//     scale: 100,
//     maxPixels: 1e13})

// print(areas) //sqm
```

RESULTS AND DISSCUSSION

CHAPTER IV
RESULTS AND DISSCUSSION

This chapter presents the findings of this study, focusing on the spatial and temporal distribution of irrigated areas in Odisha from 2018 to 2023. This chapter provides a detailed analysis of the classification accuracy of the machine learning models used, the extent of irrigated areas across different years, and the validation of these findings against agricultural statistics. The results offer insights into the effectiveness of the chosen methodologies, highlighting changes and patterns in irrigation practices over the study period. Through visual representations and statistical summaries, this chapter aims to deliver a comprehensive understanding of the changes in irrigated areas, contributing valuable information for future agricultural planning and water resource management.

4.1 Application of machine learning models for LULC classification

The first section of the results chapter presents the Land Use Land Cover (LULC) classification of the study area as determined by various machine learning (ML) models. This analysis involved the application of Random Forest (RF), Support Vector Machine (SVM), Classification and Regression Trees (CART), and Naive Bayes classifiers within Google Earth Engine (GEE). The models were trained and tested using selected bands from Sentinel-2 imagery, with training and testing datasets split 80-20%. Among the models, Random Forest proved to be the most accurate, consistently outperforming the others in classifying different land cover types, including water, agricultural land, forest, and built-up areas. The classification performance was assessed by comparing the overall accuracies of each ML model, with Random Forest emerging as the most reliable for LULC mapping in the study area. The results showcase the spatial distribution of various land cover types, laying the foundation for subsequent analysis of irrigated areas.

Fig. 4.1 illustrates a Land Use Land Cover (LULC) map of Odisha for year 2023, accompanied by a pie chart representing the proportional distribution of different land cover classes. The map visually distinguishes various land cover types across the state, with specific colours representing water bodies, agricultural land, forests, built-up areas, and other land covers. The pie chart highlights the percentage composition of each land cover class in the study area. According to the chart, the largest proportion of land cover is forests (green), accounting for 37% of the total area, followed closely by agricultural

land (yellow), which cover 35%. Built-up areas (red) make up 5% of the land, while water bodies (blue) constitute 3%. The remaining 20% (grey) is classified as other land uses. This map and chart provide a comprehensive overview of the spatial distribution and relative extent of different land cover types, offering valuable insights into the current land use patterns in Odisha. These results are crucial for understanding the dynamics of land cover change over time and for planning sustainable land management practices. The LULC map serves as a foundation for further analysis, including the examination of temporal changes in irrigated areas and their impact on land use.

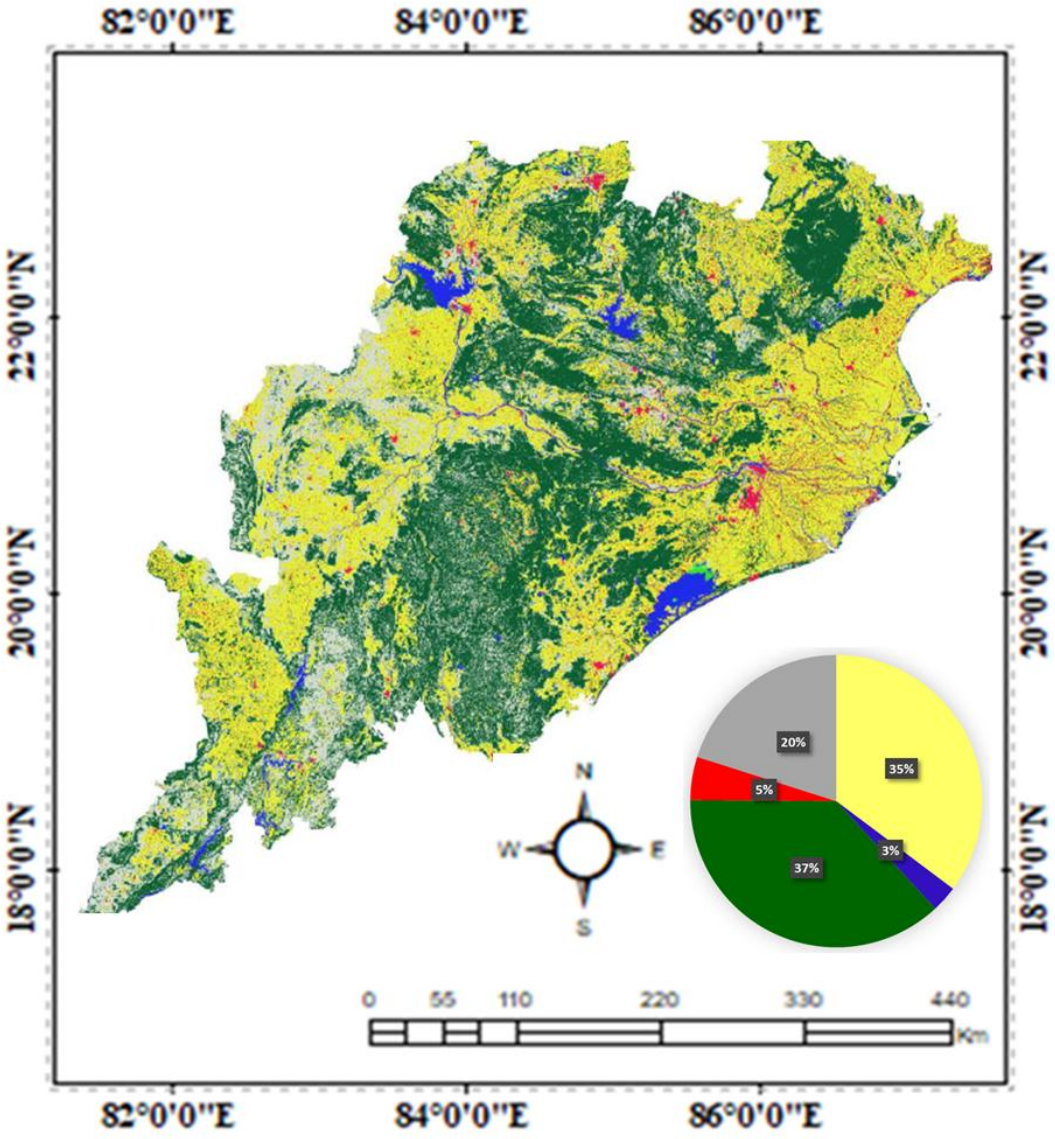

Fig. 4.1 Land Use and Land Cover Distribution in Odisha, 2023

4.1.1 Overall Accuracy of Machine Learning Models

In this study, four machine learning models were evaluated to determine the most accurate method for classifying land use and land cover (LULC) in Odisha. The models included Random Forest (RF), Classification and Regression Trees (CART), Support Vector Machine (SVM), and Naive Bayes. The overall accuracy of each model was calculated to identify the best model for the classification task.

As shown in the Fig. 4.2, the Random Forest model achieved the highest overall accuracy at 94.60%, followed by CART at 92.80%, SVM at 90.20%, and Naive Bayes at 87.50%. The high accuracy of the Random Forest model indicates that it is the most reliable model for LULC classification. Therefore, the Random Forest model was selected as the best machine learning model for the final LULC classification of the study area.

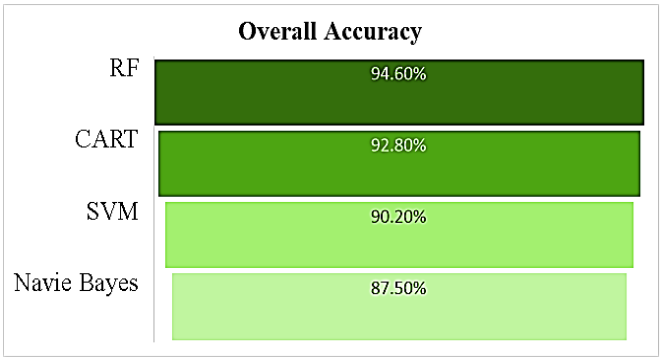

Fig. 4.2 Comparison of overall accuracy of ML models for LULC classification in Odisha

4.2 Validation of Observed and Estimated Irrigated Area

Figure 4.3 compares the observed irrigated area with the estimated irrigated area for the Rabi season of 2018 across various districts in Odisha. The observed irrigated area, represented by the dark green bars, reflects the data recorded in official agricultural statistics, while the estimated irrigated area, shown by the light green bars, is derived from the analysis conducted using Google Earth Engine (GEE).

In most districts, the estimated irrigated area closely matches the observed values, indicating a strong agreement between the GEE-derived data and the ground truth. This close alignment suggests that the methodology applied in GEE for mapping irrigated areas is effective and reliable. However, slight discrepancies is observed in some districts, which could be attributed to factors such as the resolution of satellite data, the threshold values used, or local variations in irrigation practices. Overall, the

figure demonstrates the effectiveness of the GEE-based approach in estimating irrigated areas and its potential for use in agricultural monitoring.

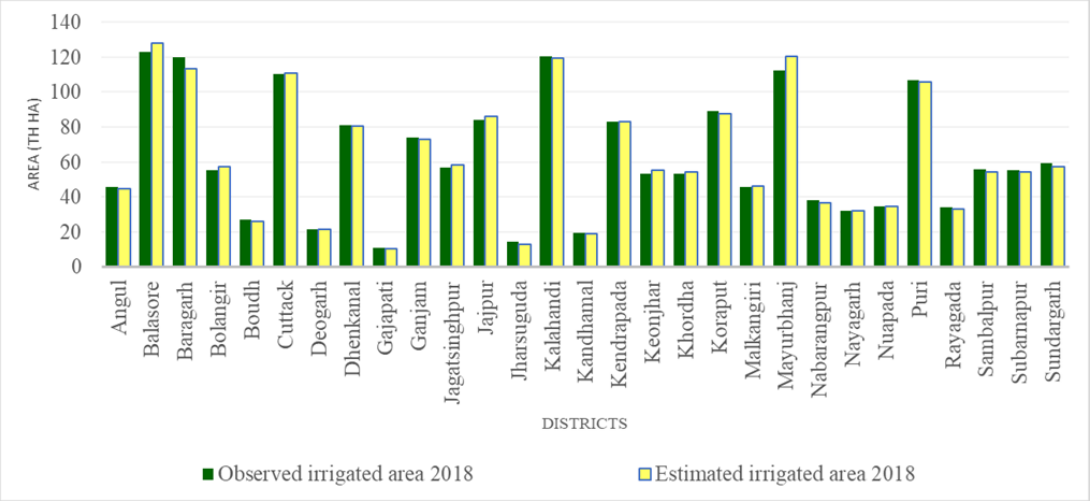

Fig. 4.3 Comparison of observed and estimated irrigated area for Rabi season in Odisha (2018)

In this section, the percentage error between observed and estimated irrigated areas for different districts during the Rabi season of 2018 was calculated. The percentage error provides insight into the accuracy of the estimation process, helping to identify the reliability of the methods used in mapping irrigated areas.

In Fig. 4.4 the percentage error between the observed and estimated irrigated areas for the districts of Odisha ranges from 0.04 to 9.7, with some districts showing minimal error and others displaying a higher discrepancy. The districts such as Kendrapada (0.04% error) and Cuttack (0.3% error) have the lowest percentage error, indicating that the estimation process is highly accurate for these regions. Moderate error districts Angul (1.8% error) and Ganjam (1.2% error) show moderate percentage errors, which are still within an acceptable range for practical purposes. Higher error districts Jharsuguda (9.7% error) and Mayurbhanj (6.7% error) exhibit relatively higher errors, suggesting that the model may require further refinement or that specific local factors may have influenced the accuracy.

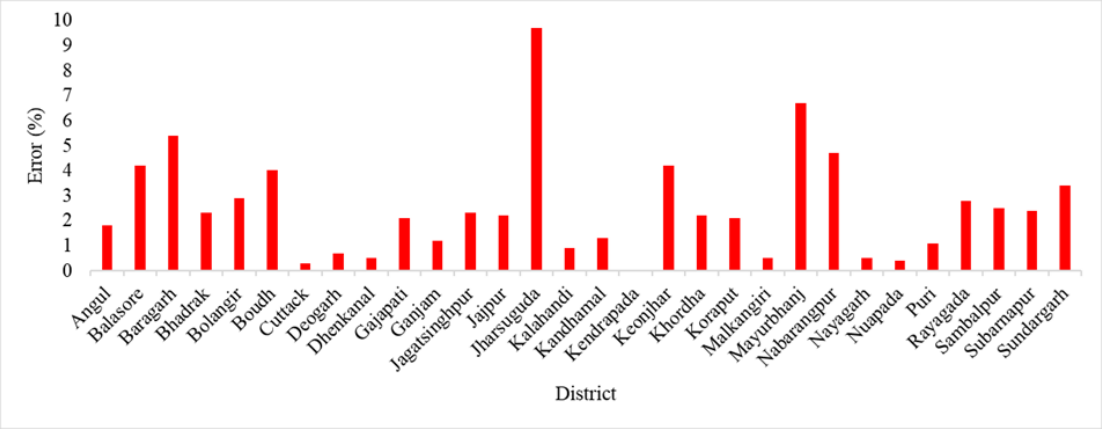

Fig. 4.4 Percentage error between observed and estimated irrigated areas for the year 2018

The overall analysis indicates that the methodology employed for estimating irrigated areas is reasonably accurate, with most districts showing minimal to moderate errors. The higher percentage errors in a few districts might be attributed to local variability in agricultural practices or environmental conditions not fully captured by the model. These findings suggest that while the model is generally reliable, further refinement could enhance its accuracy, particularly in districts with higher discrepancies. This validation process is crucial for improving future estimations and ensuring the reliability of spatial-temporal analyses of irrigated areas.

4.3 Spatio-temporal analysis of Cultivated and Irrigated Areas

Fig. 4.5 represents the comparison between the estimated cultivated area and the estimated irrigated area for the Rabi season of 2018 across various districts of Odisha. Variation across districts Balasore, Ganjam, and Kalahandi have notably higher estimated cultivated areas compared to other districts, indicating more extensive agricultural activities. Gajapati, Deogarh, and Jharsuguda show significantly lower cultivated areas, reflecting limited agricultural land and lower agricultural activity.

Balasore, Bargarh, Cuttack and Kalahandi exhibit substantial irrigated areas, highlighting the importance of irrigation in these agriculturally dominant districts. In some districts like Kalahandi and Ganjam, the irrigated area is relatively small compared to the cultivated area, suggesting reliance on rainfed agriculture and limited access to irrigation facilities.

In analysing the disparities between the estimated cultivated and irrigated areas, particularly in districts where the estimated irrigated area exceeds the estimated

cultivated area, it's important to consider potential reasons related to both the model's estimation process and the actual conditions on the ground. One possible reason for these discrepancies could be an overestimation by the model due to the presence of non-agricultural land uses (such as water bodies or wetlands) being incorrectly classified as irrigated areas. This misclassification can occur because of the spectral similarity between certain land covers in remote sensing data, which can confuse even advanced classification algorithms. Additionally, in districts with significant irrigation infrastructure, there might be scenarios where water is applied to areas not entirely dedicated to cultivation, such as fallow land being prepared for future planting or multi-cropping practices that are difficult to distinguish in seasonal data. These situations can lead to an overestimation of irrigated land relative to cultivated land. Furthermore, the model's training process, which relies on ground-truth data, might not fully capture the complexity of local agricultural practices, leading to systematic biases in the estimates.

Thus, while the overall model provides valuable insights into the spatial distribution of cultivated and irrigated areas, these discrepancies highlight the need for careful interpretation of results and consideration of local context. They also suggest areas for further refinement in model calibration, including improved ground-truthing and potentially integrating higher-resolution data or more sophisticated classification techniques. Addressing these issues can enhance the accuracy of future estimations and better support agricultural planning and water resource management in the region.

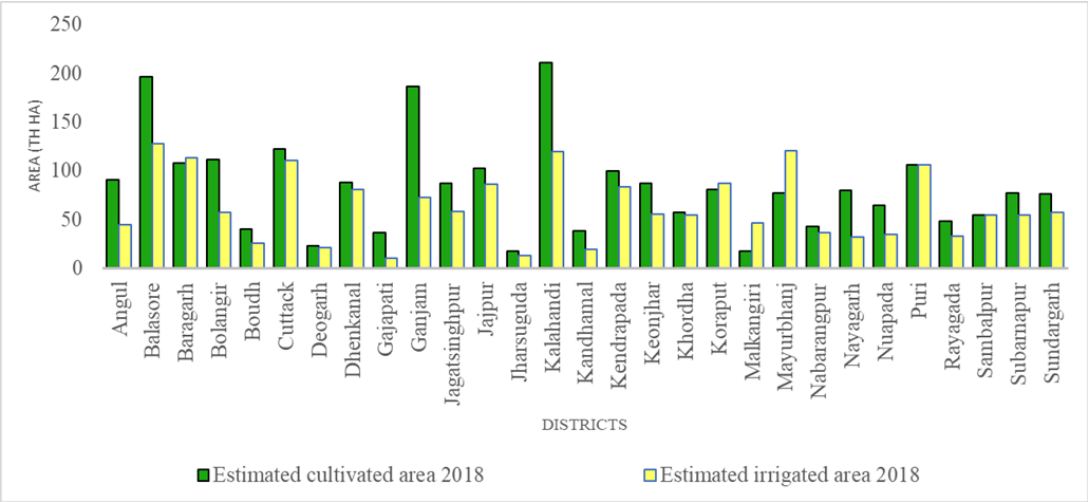

Fig. 4.5 Estimated cultivated and irrigated areas for the Rabi Season of the year2018

Fig. 4.6 presents the estimated cultivated and irrigated areas for the Rabi season of 2023 across various districts in Odisha. It provides a comparative view, highlighting the distribution and utilization of agricultural land and irrigation resources within each

district. Balasore, Baragarh, Kendrapada, Cuttack and Khordha districts show a close match between the estimated cultivated area and the irrigated area. This suggests that the irrigation infrastructure in these regions is well-developed and effectively utilized, ensuring that most of the cultivated land receives adequate water supply during the Rabi season.

In contrast, some districts show an unusual pattern where the estimated irrigated area slightly exceeds the cultivated area. This discrepancy could be due to model estimation errors, potentially arising from the misclassification of land use or overestimation of irrigated zones. It may also reflect complexities in cropping patterns or the presence of multiple crop cycles that the model might not fully account for. The disparities observed in districts underscores the ongoing challenges in irrigation infrastructure and resource allocation. Addressing these issues could lead to more equitable and effective distribution of water resources, enhancing agricultural productivity. The overestimation of irrigated areas in some districts points to the need for improved model calibration and validation. Ensuring that the model accurately reflects ground realities is crucial for making reliable agricultural assessments and planning interventions.

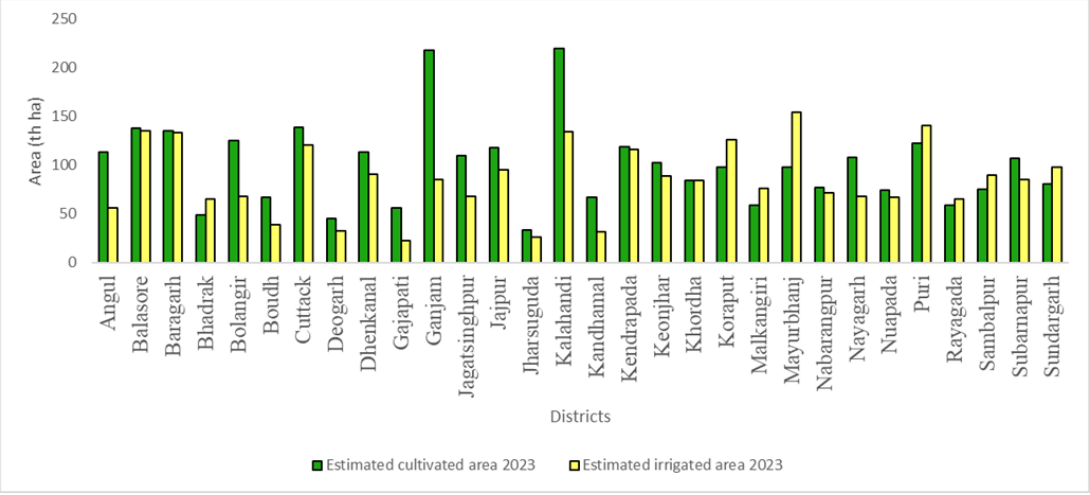

Fig. 4.6 Estimated cultivated and irrigated areas for the Rabi season of the year2023

4.3.1 Temporal Changes in Estimated Cultivated and Irrigated Areas

Fig. 4.7 presents the temporal changes in the estimated cultivated area (green) and the estimated irrigated area (yellow) for Odisha from 2018 to 2023. The data offers insights into the trends and dynamics in agricultural practices, particularly regarding the extent of land cultivation and irrigation over the observed period.

The cultivated area experienced a slight decline from 2018 to 2019. This reduction could be attributed to factors such as unfavourable weather conditions, reduced agricultural inputs, or a shift in crop selection that requires less cultivated land. But the irrigated area shows an increase from 2018 to 2019, though it remains lower than the cultivated area. This indicates that more land was brought under irrigation, possibly through expansion of irrigation infrastructure or better water management practices.

There is a significant increase in the cultivated area in 2020, marking the highest peak in the observed period. This rise might be due to enhanced agricultural practices, better rainfall, or government initiatives promoting increased cultivation. Similar to the cultivated area, the irrigated area also peaks in 2020, reflecting the increase in agricultural activities and the need for more irrigation to support the expanded cultivated area.

A slight decrease is observed in 2021 following the peak in 2020, possibly due to changes in market conditions, crop failure, or natural calamities that led to reduced cultivation. There is a noticeable decline in the irrigated area in 2021, corresponding with the decrease in the cultivated area. This decrease could be due to reduced water availability, infrastructure limitations, or a shift to crops that require less irrigation.

The cultivated area shows a steady increase from 2021 to 2023, indicating a recovery and stabilization in agricultural activities. The consistent rise suggests improvements in agricultural productivity, better resource management, or increased demand for crops. Also, the irrigated area shows a slight but steady increase, indicating efforts to expand or improve irrigation facilities in response to the growing cultivated area.

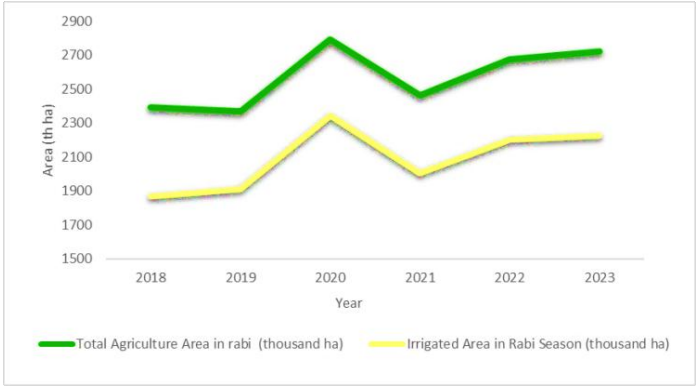

Fig. 4.7 Temporal Changes in Estimated Cultivated and Irrigated Areas from year 2018-2023

The trends in both cultivated and irrigated areas generally follow a similar pattern, suggesting a strong correlation between the two. As the cultivated area increases or decreases, the irrigated area tends to follow, reflecting the interdependence of agricultural practices and water resource management. The sharp peak in 2020 followed by a decline in 2021 may point to an exceptional year influenced by specific conditions, such as favourable weather or government policies. The subsequent decline and stabilization indicate that these conditions might not have been sustainable or that the agricultural system was adjusting to new realities.

The temporal analysis of the estimated cultivated and irrigated areas from 2018 to 2023 in Odisha reveals significant fluctuations influenced by various factors. The year 2020 stands out with the highest peak, followed by a decline and a steady recovery. The close correlation between cultivated and irrigated areas underscores the importance of synchronized agricultural and water management practices to support sustainable crop production. This analysis highlights the need for continued investment in irrigation infrastructure and adaptive strategies to maintain and enhance agricultural productivity in the region.

4.3.2 Maps of Spatio temporal distribution of Irrigated Areas

The maps illustrating the spatio-temporal distribution of irrigated areas in Odisha from 2018 to 2023, as depicted in Fig. 4.8, offer a detailed view of how irrigation practices have shifted across different districts over time. The data reveals that while top 5 districts maintained stable irrigation patterns, Cuttack as a 5th district experienced a notable transition. From 2018 to 2020, Cuttack was identified as a key irrigated region, but starting in 2021, Puri emerged as a more significant area for irrigation, replacing Cuttack in the subsequent years through to 2023. The irrigated areas for Odisha during the rabi season show fluctuations over the years, with figures of 1869.26, 1911.61, 2343.39, 2005.68, 2203.53, and 2224.53 thousand hectares for each respective year. These variations highlight not only the changes in irrigation extent due to shifts in agricultural practices and regional policies but also the adaptation of irrigation strategies to environmental conditions. The temporal analysis underscores the dynamic nature of irrigation distribution and its response to factors such as policy interventions, climate variations, and regional agricultural practices.

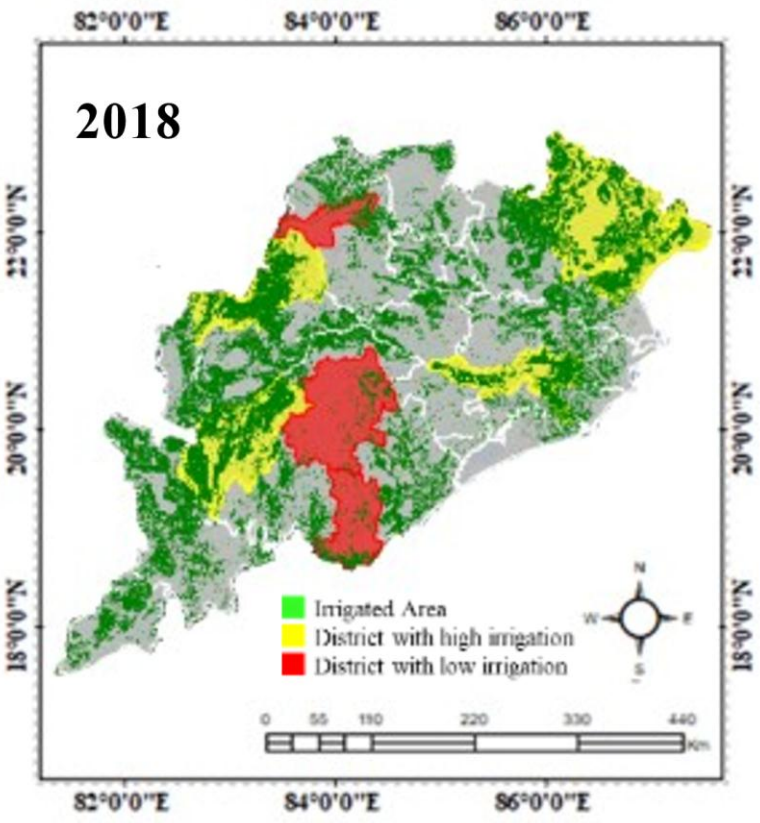
82°0'0"E
84°0'0"E
86°0'0"E
2018
22°0'0"N
20°0'0"N
18°0'0"N
Irrigated Area
District with high irrigation
District with low irrigation
N
W
E
S
0 55 110 220 330 440
Km

(a)

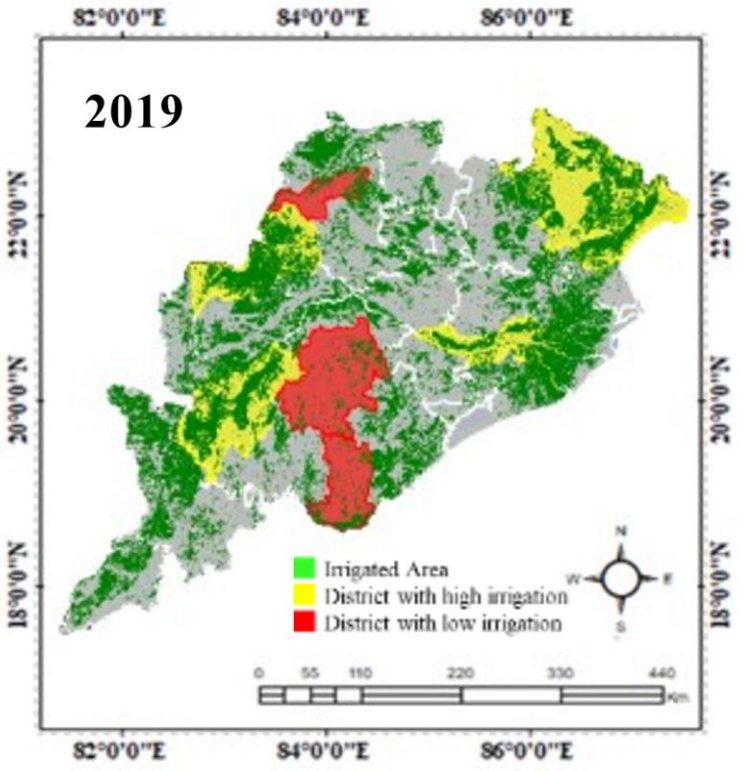
82°0'0"E
84°0'0"E
86°0'0"E
2019
22°0'0"N
20°0'0"N
18°0'0"N
Irrigated Area
District with high irrigation
District with low irrigation
N
W
E
S
0 55 110 220 330 440
Km

(b)

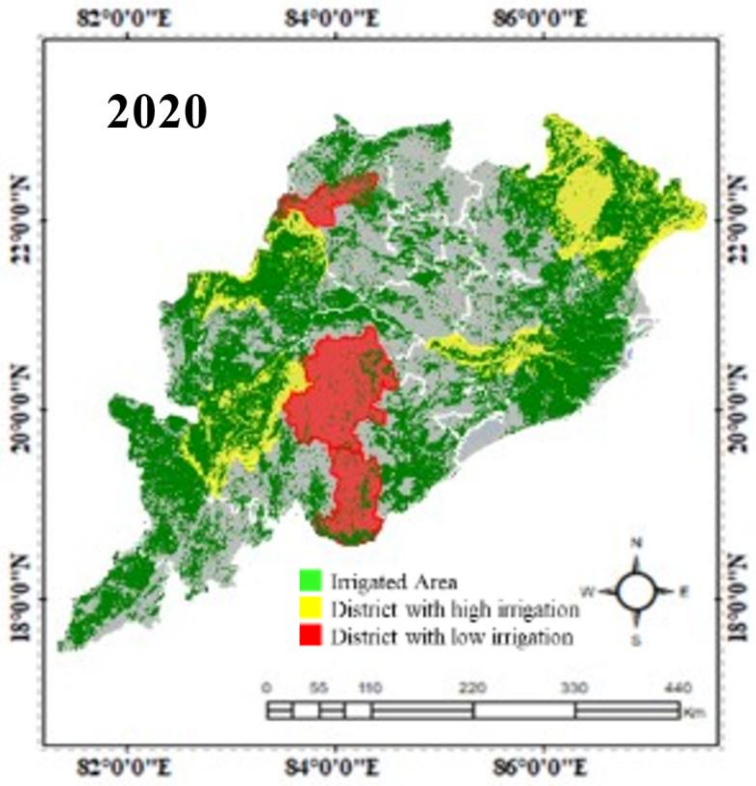
2020
82°0'0"E
84°0'0"E
86°0'0"E
22°0'0"N
20°0'0"N
18°0'0"N
Irrigated Area
District with high irrigation
District with low irrigation
N
W
E
S
0
55
110
220
330
440
Km

(c)

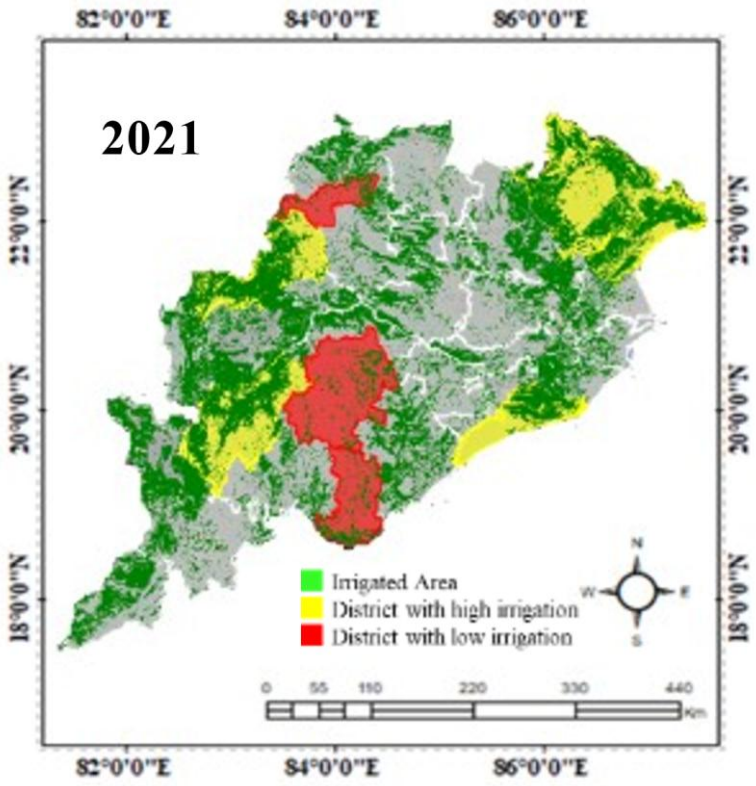
2021
82°0'0"E
84°0'0"E
86°0'0"E
22°0'0"N
20°0'0"N
18°0'0"N
Irrigated Area
District with high irrigation
District with low irrigation
N
W
E
S
0
55
110
220
330
440
Km

(d)

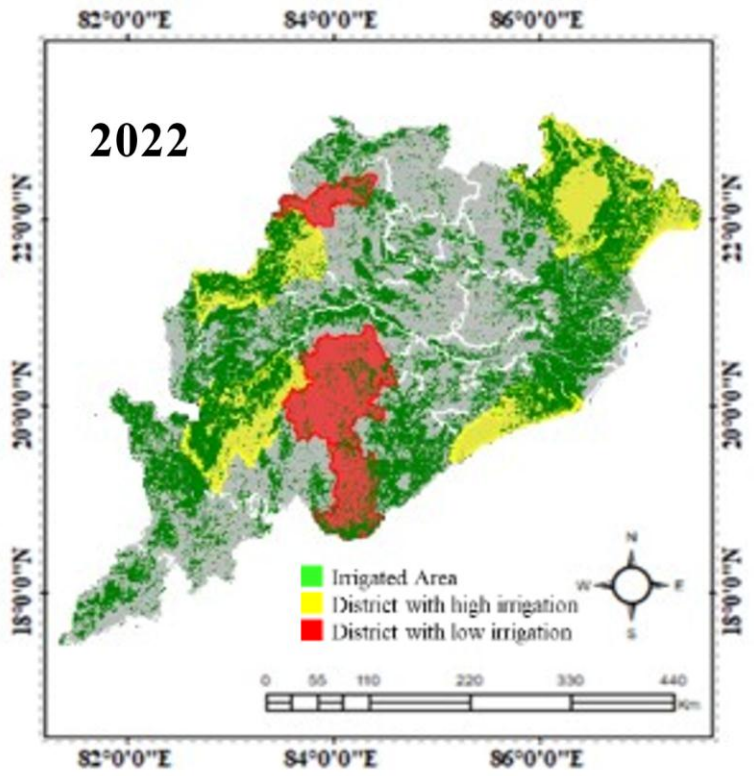

(e)

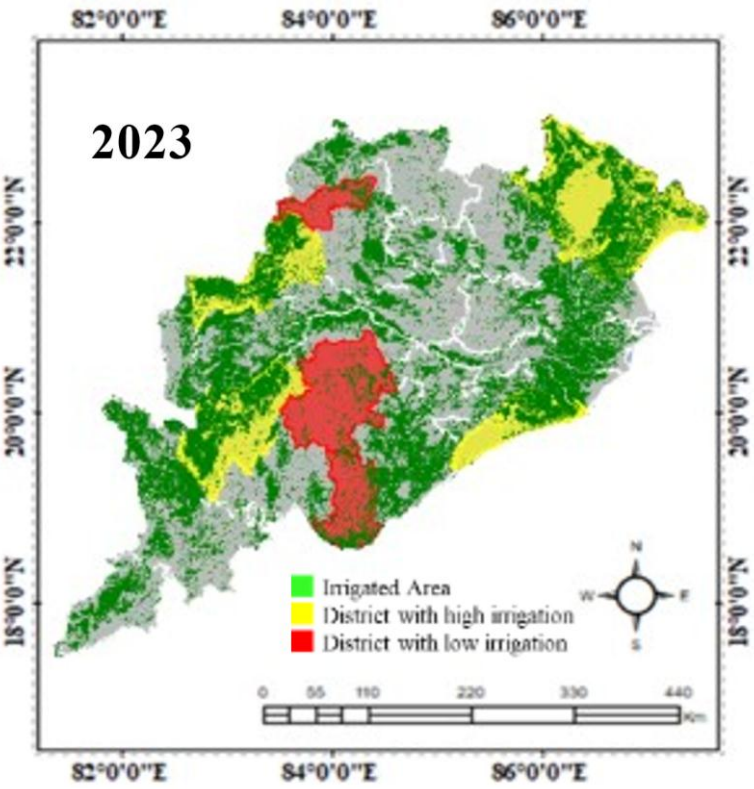

(f)

Fig. 4.8 Maps showing spatial and temporal distribution of Irrigated Areas from year 2018 to 2023

SUMMARY AND CONCLUSION

CHAPTER V
SUMMARY AND CONCLUSION

5.1 Summary

This chapter provides an overview of the study area, data utilized, and the methodology employed in this research. The study area is Odisha, located between 17° 49' 25" to 22° 34' 30" N latitude and 81° 27' 35" to 87° 29' 30" E longitude, characterized by a diverse agricultural landscape and a climate with temperatures ranging from 10°C to 40°C, with peaks up to 45°C. Annual rainfall varies between 1200 mm to 1800 mm, and the soil is predominantly red and laterite, with some areas of black soil. The state's agricultural economy is significant, with major crops including rice, pulses, oilseeds, and cotton. The total cultivated land is 61.80 lakh hectares, of which 65% is irrigated. The study area encompasses 30 districts, each contributing to the agricultural diversity of the state.

The data used in the study include Sentinel-2 data for Land Use Land Cover (LULC) mapping, NDVI data for assessing vegetation, FAO data for administrative boundaries, and irrigation data for validation from 2018. Sentinel-2 data, with a spatial resolution of 10 meters and a temporal resolution of 5 days, were used to create LULC maps, utilizing various spectral bands like Blue, Green, Red, NIR, Red Edge, and SWIR. Landsat-8 data, with a spatial resolution of 30 meters and a temporal resolution of 16 days, was used to calculate NDVI, with the Red and Near-Infrared bands. FAO data was employed to extract district boundaries for spatial analysis, while the 2018 irrigation data provided by the Government of Odisha was used to validate the estimated irrigated areas.

The methodology involved evaluating machine learning models in Google Earth Engine (GEE) to map irrigated areas and estimate their spatio-temporal distribution from 2018 to 2023. Sentinel-2 data was processed by applying cloud masks and atmospheric corrections, and temporal composites were created to obtain cloud-free imagery. Ground truth data for LULC classification was collected by plotting visual datasets, and various machine learning models, including Random Forest, Support Vector Machine, Classification and Regression Trees, and Naive Bayes, were trained on these features. The models were trained using 80% of the data, with 20% reserved for testing. This process allowed for accurate classification of land cover into four distinct categories: water, agriculture, forest, and built-up areas. The accuracy of the mapping

was validated using the 2018 irrigation data, ensuring that the results were reliable and reflective of the actual conditions in Odisha during the study period.

5.2 Conclusion

In conclusion, the application of machine learning models in mapping irrigated areas in Odisha using Google Earth Engine (GEE) has proven highly effective, with the Random Forest (RF) classifier demonstrating an accuracy of 94.60%, surpassing other models. By utilizing visual points plotted in GEE, a land use/land cover (LULC) map of Odisha was successfully extracted, and agricultural land was further delineated. The NDVI threshold range of 0.4 to 0.7 was applied to estimate district-wise irrigated areas during the Rabi season. These estimates were compared with observed values provided by the Government of Odisha, revealing a strong alignment in most districts. The calculated percentage error between observed and estimated values ranged from 0.04% to 9.7%, with districts such as Kendrapada (0.04% error) and Cuttack (0.3% error) exhibiting minimal discrepancies. However, higher errors were observed in districts like Jharsuguda (9.7% error) and Mayurbhanj (6.7% error), suggesting potential areas for model refinement or the influence of local factors. The close agreement between GEE-derived data and ground truth underscores the reliability of the applied methodology for mapping irrigated areas.

The spatio-temporal analysis of cultivated and irrigated areas from 2018 to 2023 provides valuable insights into the agricultural dynamics across Odisha. Notable variations were observed, with districts like Balasore, Ganjam, and Kalahandi displaying higher cultivated areas, reflecting intensive agricultural activities, while Gajapati, Deogarh, and Jharsuguda exhibited lower cultivation. Irrigation's critical role is highlighted in districts such as Balasore, Bargarh, Cuttack, and Kalahandi, where substantial irrigated areas were recorded. Temporal analysis revealed fluctuations in both cultivated and irrigated areas, with a significant increase in 2020, likely due to favourable conditions and government initiatives. Although a slight decline followed in 2021, the period from 2021 to 2023 saw a steady recovery in cultivated areas, paralleled by a consistent rise in irrigated land, indicating ongoing efforts to enhance agricultural productivity and irrigation infrastructure. This comprehensive analysis, supported by spatio-temporal maps of irrigated areas, provides a robust foundation for understanding the agricultural landscape of Odisha and underscores the effectiveness of GEE and RF models in monitoring and managing irrigated agriculture over time.

5.3 Suggestions for Future Work

- This study can be carried out using deep learning models to enhance classification.
- This study can also examine the effects of irrigation on crop yield and water resources.

REFERENCES

REFERENCES

Alencar, A., Shimbo, J. Z., Lenti, F., Marques, C. B., Zimbres, B., Rosa, M., Arruda, V., Castro, I., Ribeiro, J. P. F. M., Varela, V., Alencar, I., Piontekowski, V., Ribeiro, V., Bustamante, M. M. C., Sano, E. E., & Barroso, M. (2020). Mapping three decades of changes in the brazilian savanna native vegetation using landsat data processed in the google earth engine platform. Remote Sensing, 12(6). https://doi.org/10.3390/rs12060924

Amani, M., Ghorbanian, A., Ahmadi, S. A., Kakooei, M., Moghimi, A., Mirmazloumi, S. M., Moghaddam, S. H. A., Mahdavi, S., Ghahremanloo, M., Parsian, S., Wu, Q., & Brisco, B. (2020). Google Earth Engine Cloud Computing Platform for Remote Sensing Big Data Applications: A Comprehensive Review. IEEE Journal of Selected Topics in Applied Earth Observations and Remote Sensing, 13. https://doi.org/10.1109/JSTARS.2020.3021052

Angelakis, A. N., Zaccaria, D., Krasilnikoff, J., Salgot, M., Bazza, M., Roccaro, P., Jimenez, B., Kumar, A., Yinghua, W., Baba, A., Harrison, J. A., Garduno-Jimenez, A., & Fereres, E. (2020). Irrigation of world agricultural lands: Evolution through the Millennia. In Water (Switzerland) (Vol. 12, Issue 5). https://doi.org/10.3390/W12051285

Arpitha, M., Ahmed, S. A., & Harishnaika, N. (2023). Land use and land cover classification using machine learning algorithms in google earth engine. In Earth Science Informatics (Vol. 16, Issue 4). https://doi.org/10.1007/s12145-023-01073-w

Basukala, A. K., Oldenburg, C., Schellberg, J., Sultanov, M., & Dubovyk, O. (2017). Towards improved land use mapping of irrigated croplands: performance assessment of different image classification algorithms and approaches. European Journal of Remote Sensing, 50(1). https://doi.org/10.1080/22797254.2017.1308235

Denby, K., Movik, S., Mehta, L., & van Koppen, B. (2016). The “trickle down” of IWRM: A case study of local-level realities in the Inkomati Water Management Area, South Africa. Water Alternatives, 9(3).

du Plessis, A. (2019). Current Water Quality Risk Areas for Limpopo, Olifants and the Inkomati-Usuthu WMAs. In Springer Water. https://doi.org/10.1007/978-3-030-03186-2_9

Gumma, M. K., Thenkabail, P. S., Teluguntla, P. G., Oliphant, A., Xiong, J., Giri, C., Pyla, V., Dixit, S., & Whitbread, A. M. (2020). Agricultural cropland extent and areas of South Asia derived using Landsat satellite 30-m time-series big-data using random forest machine learning algorithms on the Google Earth Engine cloud. GIScience and Remote Sensing, 57(3). https://doi.org/10.1080/15481603.2019.1690780

Han, J., Zhang, Z., Cao, J., Luo, Y., Zhang, L., Li, Z., & Zhang, J. (2020). Prediction of winter wheat yield based on multi-source data and machine learning in China. Remote Sensing, 12(2). https://doi.org/10.3390/rs12020236

Latif, R. M. A., He, J., & Umer, M. (2023). Mapping Cropland Extent in Pakistan Using Machine Learning Algorithms on Google Earth Engine Cloud Computing Framework. ISPRS International Journal of Geo-Information, 12(2). https://doi.org/10.3390/ijgi12020081

Magidi, J., Nhamo, L., Mpandeli, S., & Mabhaudhi, T. (2021). Application of the random forest classifier to map irrigated areas using google earth engine. Remote Sensing, 13(5), 1–15. https://doi.org/10.3390/rs13050876

Meier, J., Zabel, F., & Mauser, W. (2018). A global approach to estimate irrigated areas - A comparison between different data and statistics. Hydrology and Earth System Sciences, 22(2). https://doi.org/10.5194/hess-22-1119-2018

Nhamo, L., Magidi, J., Nyamugama, A., Clulow, A. D., Sibanda, M., Chimonyo, V. G. P., & Mabhaudhi, T. (2020). Prospects of improving agricultural and water productivity through unmanned aerial vehicles. In Agriculture (Switzerland) (Vol. 10, Issue 7). https://doi.org/10.3390/agriculture10070256

Nhamo, L., van Dijk, R., Magidi, J., Wiberg, D., & Tshikolomo, K. (2018). Improving the accuracy of remotely sensed irrigated areas using post-classification enhancement through UAV capability. Remote Sensing, 10(5). https://doi.org/10.3390/rs10050712

Nhemachena, C., Nhamo, L., Matchaya, G., Nhemachena, C. R., Muchara, B., Karuaihe, S. T., & Mpandeli, S. (2020). Climate change impacts on water and agriculture sectors in southern africa: Threats and opportunities for sustainable development. In Water (Switzerland) (Vol. 12, Issue 10). https://doi.org/10.3390/w12102673

Pandey, A. C., Kaushik, K., & Parida, B. R. (2022). Google Earth Engine for Large-Scale Flood Mapping Using SAR Data and Impact Assessment on Agriculture and Population of Ganga-Brahmaputra Basin. Sustainability (Switzerland), 14(7). https://doi.org/10.3390/su14074210

Phiri, D., Simwanda, M., Salekin, S., Nyirenda, V. R., Murayama, Y., & Ranagalage, M. (2020). Sentinel-2 data for land cover/use mapping: A review. In Remote Sensing (Vol. 12, Issue 14). https://doi.org/10.3390/rs12142291

Portmann, F. T., Siebert, S., & Döll, P. (2010). MIRCA2000—Global monthly irrigated and rainfed crop areas around the year 2000: A new high□resolution data set for agricultural and hydrological modeling. Global Biogeochemical Cycles, 24(1). https://doi.org/10.1029/2008gb003435

Rayne, L., Brandolini, F., Makovics, J. L., Hayes-Rich, E., Levy, J., Irvine, H., Assi, L., & Bokbot, Y. (2023). Detecting desertification in the ancient oases of southern Morocco. Scientific Reports, 13(1). https://doi.org/10.1038/s41598-023-46319-1

Riddell, E. S., Govender, D., Botha, J., Sithole, H., Petersen, R. M., & Shikwambana, P. (2019). Pollution impacts on the aquatic ecosystems of the Kruger National Park, South Africa. Scientific African, 6. https://doi.org/10.1016/j.sciaf.2019.e00195

Saad El Imanni, H., El Harti, A., Hssaisoune, M., Velastegui-Montoya, A., Elbouzidi, A., Addi, M., El Iysaouy, L., & El Hachimi, J. (2022). Rapid and Automated Approach for Early Crop Mapping Using Sentinel-1 and Sentinel-2 on Google Earth Engine; A Case of a Highly Heterogeneous and Fragmented Agricultural Region. Journal of Imaging, 8(12). https://doi.org/10.3390/jimaging8120316

Teluguntla, P., Thenkabail, P., Oliphant, A., Xiong, J., Gumma, M. K., Congalton, R. G., Yadav, K., & Huete, A. (2018). A 30-m landsat-derived cropland extent

product of Australia and China using random forest machine learning algorithm on Google Earth Engine cloud computing platform. ISPRS Journal of Photogrammetry and Remote Sensing, 144. https://doi.org/10.1016/j.isprsjprs.2018.07.017

Thenkabail, P. S., Dheeravath, V., Biradar, C. M., Gangalakunta, O. R. P., Noojipady, P., Gurappa, C., Velpuri, M., Gumma, M., & Li, Y. (2009). Irrigated area maps and statistics of India using remote sensing and national statistics. Remote Sensing, 1(2). https://doi.org/10.3390/rs1020050

Thenkabail, P. S., GangadharaRao, P., Biggs, T. W., Krishna, M., & Turral, H. (2007). Spectral matching techniques to determine historical Land-use/Land-cover (LULC) and irrigated areas using time-series 0.1-degree AVHRR pathfinder datasets. Photogrammetric Engineering and Remote Sensing, 73(9).

Tian, H., Huang, N., Niu, Z., Qin, Y., Pei, J., & Wang, J. (2019). Mapping winter crops in China with multi-source satellite imagery and phenology-based algorithm. Remote Sensing, 11(7). https://doi.org/10.3390/rs11070820

Torbick, N., Chowdhury, D., Salas, W., & Qi, J. (2017). Monitoring Rice Agriculture across Myanmar Using Time Series Sentinel-1 Assisted by Landsat-8 and PALSAR-2. Remote Sensing, 9(2). https://doi.org/10.3390/rs9020119

Velastegui-Montoya, A., Montalván-Burbano, N., Carrión-Mero, P., Rivera-Torres, H., Sadeck, L., & Adami, M. (2023). Google Earth Engine: A Global Analysis and Future Trends. In Remote Sensing (Vol. 15, Issue 14). https://doi.org/10.3390/rs15143675

Venkatappa, M., Sasaki, N., Shrestha, R. P., Tripathi, N. K., & Ma, H. O. (2019). Determination of vegetation thresholds for assessing land use and land use changes in Cambodia using the Google Earth Engine cloud-computing platform. Remote Sensing, 11(13). https://doi.org/10.3390/rs11131514

Waleed, M., Mubeen, M., Ahmad, A., Habib-ur-Rahman, M., Amin, A., Farid, H. U., Hussain, S., Ali, M., Qaisrani, S. A., Nasim, W., Javeed, H. M. R., Masood, N., Aziz, T., Mansour, F., & EL Sabagh, A. (2022). Evaluating the efficiency of coarser to finer resolution multispectral satellites in mapping paddy rice fields

using GEE implementation. Scientific Reports, 12(1). https://doi.org/10.1038/s41598-022-17454-y

Xiong, J., Thenkabail, P. S., Tilton, J. C., Gumma, M. K., Teluguntla, P., Oliphant, A., Congalton, R. G., Yadav, K., & Gorelick, N. (2017). Nominal 30-m cropland extent map of continental Africa by integrating pixel-based and object-based algorithms using Sentinel-2 and Landsat-8 data on google earth engine. Remote Sensing, 9(10). https://doi.org/10.3390/rs9101065

Yang, L., Driscol, J., Sarigai, S., Wu, Q., Chen, H., & Lippitt, C. D. (2022). Google Earth Engine and Artificial Intelligence (AI): A Comprehensive Review. In Remote Sensing (Vol. 14, Issue 14). https://doi.org/10.3390/rs14143253

Zhang, C., Dong, J., Xie, Y., Zhang, X., & Ge, Q. (2022). Mapping irrigated croplands in China using a synergetic training sample generating method, machine learning classifier, and Google Earth Engine. International Journal of Applied Earth Observation and Geoinformation, 112. https://doi.org/10.1016/j.jag.2022.102888

Zohaib, M., Kim, H., & Choi, M. (2019). Detecting global irrigated areas by using satellite and reanalysis products. Science of the Total Environment, 677. https://doi.org/10.1016/j.scitotenv.2019.04.365

Zurqani, H. A., Allen, J. S., Post, C. J., Pellett, C. A., & Walker, T. C. (2021). Mapping and quantifying agricultural irrigation in heterogeneous landscapes using Google Earth Engine. Remote Sensing Applications: Society and Environment, 23. https://doi.org/10.1016/j.rsase.2021.100590

Ambika, A. K., Wardlow, B., & Mishra, V. (2016). Remotely sensed high resolution irrigated area mapping in India for 2000 to 2015. Scientific Data, 3. https://doi.org/10.1038/sdata.2016.118

Magidi, J., Nhamo, L., Mpandeli, S., & Mabhaudhi, T. (2021). Application of the random forest classifier to map irrigated areas using google earth engine. Remote Sensing, 13(5), 1–15. https://doi.org/10.3390/rs13050876

Dong, J., Xiao, X., Menarguez, M. A., Zhang, G., Qin, Y., Thau, D., Biradar, C., & Moore, B. (2016). Mapping paddy rice planting area in northeastern Asia with

Landsat 8 images, phenology-based algorithm and Google Earth Engine. Remote Sensing of Environment, 185. https://doi.org/10.1016/j.rse.2016.02.016

Hemati, M., Hasanlou, M., Mahdianpari, M., & Mohammadimanesh, F. (2021). A systematic review of landsat data for change detection applications: 50 years of monitoring the earth. In Remote Sensing (Vol. 13, Issue 15). https://doi.org/10.3390/rs13152869

Liu, C. C., Shieh, M. C., Ke, M. S., & Wang, K. H. (2018). Flood prevention and emergency response system powered by Google Earth Engine. In Remote Sensing (Vol. 10, Issue 8). https://doi.org/10.3390/rs10081283

Mandal, D., Kumar, V., Bhattacharya, A., & Rao, Y. S. (2017). Monitoring rice crop using time series sentinel-1 data in google earth engine platform. 38th Asian Conference on Remote Sensing - Space Applications: Touching Human Lives, ACRS 2017, 2017-October.

Markert, K. N., Schmidt, C. M., Griffin, R. E., Flores, A. I., Poortinga, A., Saah, D. S., Muench, R. E., Clinton, N. E., Chishtie, F., Kityuttachai, K., Someth, P., Anderson, E. R., Aekakkararungroj, A., & Ganz, D. J. (2018). Historical and operational monitoring of surface sediments in the Lower Mekong Basin using Landsat and Google Earth Engine cloud computing. Remote Sensing, 10(6). https://doi.org/10.3390/rs10060909

Pham-Duc, B., & Nguyen, H. (2022). A bibliometric analysis on the visibility of the Sentinel-1 mission in the scientific literature. Arabian Journal of Geosciences, 15(9). https://doi.org/10.1007/s12517-022-10089-3

Rosegrant, M. W., & Cline, S. A. (2003). Global Food Security: Challenges and Policies. In Science (Vol. 302, Issue 5652). https://doi.org/10.1126/science.1092958

Sazib, N., Mladenova, I., & Bolten, J. (2018). Leveraging the google earth engine for drought assessment using global soil moisture data. Remote Sensing, 10(8). https://doi.org/10.3390/rs10081265

Taghizadeh-Mehrjardi, R., Schmidt, K., Amirian-Chakan, A., Rentschler, T., Zeraatpisheh, M., Sarmadian, F., Valavi, R., Davatgar, N., Behrens, T., &

Scholten, T. (2020). Improving the spatial prediction of soil organic carbon content in two contrasting climatic regions by stacking machine learning models and rescanning covariate space. Remote Sensing, 12(7). https://doi.org/10.3390/rs12071095

Tamiminia, H., Salehi, B., Mahdianpari, M., Quackenbush, L., Adeli, S., & Brisco, B. (2020). Google Earth Engine for geo-big data applications: A meta-analysis and systematic review. In ISPRS Journal of Photogrammetry and Remote Sensing (Vol. 164). https://doi.org/10.1016/j.isprsjprs.2020.04.001

Tian, H., Huang, N., Niu, Z., Qin, Y., Pei, J., & Wang, J. (2019). Mapping winter crops in China with multi-source satellite imagery and phenology-based algorithm. Remote Sensing, 11(7). https://doi.org/10.3390/rs11070820

Tsai, Y. H., Stow, D., Chen, H. L., Lewison, R., An, L., & Shi, L. (2018). Mapping vegetation and land use types in Fanjingshan National Nature Reserve using google earth engine. Remote Sensing, 10(6). https://doi.org/10.3390/rs10060927

Wang, X., Huang, J., Feng, Q., & Yin, D. (2020). Winter wheat yield prediction at county level and uncertainty analysis in main wheat-producing regions of China with deep learning approaches. Remote Sensing, 12(11). https://doi.org/10.3390/rs12111744

Zhao, Q., Yu, L., Li, X., Peng, D., Zhang, Y., & Gong, P. (2021). Progress and trends in the application of google earth and google earth engine. In Remote Sensing (Vol. 13, Issue 18). https://doi.org/10.3390/rs13183778

APPENDICES

Table 1. LULC of Odisha for year 2023

LULC	Area (sq km)
Agriculture land	53955.9
Water bodies	4446.04
Forest	56639.94
Built-up	7319.83
Bare ground and rangeland	30785.16

Table 2. List of ML models showing Overall Accuracy

ML Models	Overall Accuracy
RF	94.60%
CART	92.80%
SVM	90.20%
Navie Bayes	87.50%

Table 3. District wise estimated area for year 2018 -2020

Districts	Estimated Area 2018		Estimated Area 2019		Estimated Area 2020	
	Total Area (th ha)	Irrigated Area (th ha)	Total Area (th ha)	Irrigated Area (th ha)	Total Area (th ha)	Irrigated Area (th ha)
Angul	90.21	44.84	93.85	46.81	106.19	60.06
Balasore	195.83	127.88	154.09	124.5	169.87	138.58
Baragarh	107.22	113.3	109.02	124.17	127.94	137.08
Bhadrak	24.99	53.79	28.78	53.36	40.03	68.5
Bolangir	111.35	57.15	103.34	57.91	117,4	71.58
Boudh	40.11	25.95	42.09	27.86	59.25	42.36
Cuttack	122.47	110.71	121.26	111.26	131.79	124.59
Deogarh	23.05	21.26	24.47	21.74	37.84	35.9
Dhenkanal	87.86	80.53	90.34	81.69	106.85	94.68
Gajapati	36.65	10.52	37.71	10.88	47.55	26.1
Ganjam	186.13	72.77	197.56	75.1	210.64	88.85
Jagatsinghpur	87	58.15	86.08	57.16	101.9	71.74
Jajpur	102.36	86.14	92.18	85.54	111.14	98.95
Jharsuguda	17.29	12.902	14.44	15.5	25.74	29.74
Kalahandi	210.87	119.51	199.41	124.38	213.55	137.45
Kandhamal	38.42	18.91	41.66	19.71	58.94	35.01
Kendrapada	99.86	83.23	101.6	83.96	112.22	97.79
Keonjhar	86.57	55.48	81.64	54.36	95.1	69.02
Khordha	57.4	54.27	61.22	53.55	77.82	67.04
Koraput	80.81	87.32	80.13	92.59	90.07	106.91
Malkangiri	17.66	46.07	39.5	45.99	52,28	59.14
Mayurbhanj	76.54	120.19	73.53	117.87	89.45	133.25
Nabarangpur	42.6	36.49	50.62	39.42	69.68	53.33
Nayagarh	79.93	32.02	88.65	32.92	100.05	47.66
Nuapada	64.28	34.44	53.01	35.65	67.25	49.22
Puri	106.13	105.52	97.45	107.16	114.83	121.56
Rayagada	48.28	33.12	41.12	35.21	51.84	48.44
Sambalpur	54.3	54.22	54.36	56.95	67.92	71.01
Subarnapur	76.92	54.05	84.97	56.09	101.67	68.98
Sundargarh	75.89	57.28	76.13	62.2	72.19	77.32
Total	**2348.98**	**1868.14**	**2370.21**	**1911.61**	**2791.61**	**2343.39**

Table 4. District wise estimated area for year 2021 -2023

Districts	Estimated Area 2021		Estimated Area 2022		Estimated Area 2023	
	Total Area (th ha)	Irrigated Area (th ha)	Total Area (th ha)	Irrigated Area (th ha)	Total Area (th ha)	Irrigated Area (th ha)
Angul	105.74	49.81	112.06	55.73	113.31	56.38
Balasore	129.09	127.5	136.21	134.25	137.69	135.03
Baragarh	126.92	127.17	132.9	132.75	134.61	133.26
Bhadrak	39.78	56.36	47.99	64.17	48.93	65.01
Bolangir	116.84	60.91	123.58	67.25	124.75	67.92
Boudh	58.36	30.86	65.93	38.03	67.33	38.83
Cuttack	131.66	114.26	138.06	120.26	138.69	120.89
Deogarh	37.37	24.74	44.6	31.57	45.46	32.33
Dhenkanal	106.14	84.69	112.2	90.35	113.29	90.94
Gajapati	47.51	13.88	55.8	21.77	56.12	22.59
Ganjam	210.26	78.1	217.08	84.52	217.63	85.17
Jagatsinghpur	101.28	60.16	108.93	67.41	109.79	68.19
Jajpur	110.28	88.54	116.76	94.62	117.77	95.23
Jharsuguda	25.64	18.5	32.95	25.41	33.19	26.15
Kalahandi	213.11	127.38	219.25	133.12	219.72	133.69
Kandhamal	58.16	22.71	66.53	30.68	67.23	31.48
Kendrapada	112.1	108.62	119	115.12	119.03	115.75
Keonjhar	94.64	80.68	102.37	88.01	102.63	88.77
Khordha	77.12	77.53	83.68	83.69	84.17	84.28
Koraput	89.98	118.23	97.37	125.22	97.49	126.04
Malkangiri	51.95	69.29	58.17	75.11	58,52	75.76
Mayurbhanj	88.88	145.63	97.33	153.68	97.91	154.46
Nabarangpur	68.87	64.24	75.85	70.82	76.66	71.43
Nayagarh	99.9	59.4	107.71	66.81	107.85	67.55
Nuapada	66.76	59.79	73.4	66.03	73.77	66.6
Puri	114	132.96	121.47	140.03	122.07	140.83
Rayagada	51.67	58.67	57.97	64.57	58.8	65.2
Sambalpur	67.41	82.07	74.54	88.8	74.7	89.56
Subarnapur	100.92	78.87	106.88	84.43	107.27	85.02
Sundargarh	72.08	89.44	80.27	97.23	80.89	98.05
Total	**2465.12**	**2005.68**	**2674.86**	**2203.53**	**2722.17**	**2224.53**

Table 5. District wise observed and estimated area for year 2018

Districts	Observed Area 2018		Estimated Area 2018	
	Total Area (th ha)	Irrigated Area (th ha)	Total Area (th ha)	Irrigated Area (th ha)
Angul	87.14	45.7	90.21	44.84
Balasore	194.22	122.7	195.83	127.88
Baragarh	113.82	119.81	107.22	113.3
Bhadrak	32.21	52.57	24.99	53.79
Bolangir	107.86	55.49	111.35	57.15
Boudh	45.47	27.04	40.11	25.95
Cuttack	125.97	110.37	122.47	110.71
Deogarh	27.88	21.42	23.05	21.26
Dhenkanal	93.06	80.98	87.86	80.53
Gajapati	40.14	10.75	36.65	10.52
Ganjam	193.02	73.69	186.13	72.77
Jagatsinghpur	94.26	56.79	87	58.15
Jajpur	90.75	84.22	102.36	86.14
Jharsuguda	21.64	14.29	17.29	12.902
Kalahandi	196.42	120.65	210.87	119.51
Kandhamal	36.72	19.17	38.42	18.91
Kendrapada	96.18	83.19	99.86	83.23
Keonjhar	86.31	53.23	86.57	55.48
Khordha	63.21	53.06	57.4	54.27
Koraput	78.94	89.27	80.81	87.32
Malkangiri	20.57	45.84	17.66	46.07
Mayurbhanj	79.36	112.54	76.54	120.19
Nabarangpur	50.83	38.3	42.6	36.49
Nayagarh	86.58	32.21	79.93	32.02
Nuapada	64.94	34.58	64.28	34.44
Puri	102.65	106.7	106.13	105.52
Rayagada	48.14	34.09	48.28	33.12
Sambalpur	56.75	55.63	54.3	54.22
Subarnapur	88.75	55.38	76.92	54.05
Sundargarh	67.08	59.33	75.89	57.28
Total	**2390.87**	**1869.26**	**2348.98**	**1868.14**

Table 6. District wise percentage error for observed and estimated area (2018)

District	Observed irrigated area 2018	Estimated irrigated area 2018	Percentage Error
Angul	45.7	44.84	1.8
Balasore	122.7	127.88	4.2
Baragarh	119.81	113.3	5.4
Bhadrak	52.57	53.79	2.3
Bolangir	55.49	57.15	2.9
Boudh	27.04	25.95	4.0
Cuttack	110.37	110.71	0.3
Deogarh	21.42	21.26	0.7
Dhenkanal	80.98	80.53	0.5
Gajapati	10.75	10.52	2.1
Ganjam	73.69	72.77	1.2
Jagatsinghpur	56.79	58.15	2.3
Jajpur	84.22	86.14	2.2
Jharsuguda	14.29	12.902	9.7
Kalahandi	120.65	119.51	0.9
Kandhamal	19.17	18.91	1.3
Kendrapada	83.19	83.23	0.04
Keonjhar	53.23	55.48	4.2
Khordha	53.06	54.27	2.2
Koraput	89.27	87.32	2.1
Malkangiri	45.84	46.07	0.5
Mayurbhanj	112.54	120.19	6.7
Nabarangpur	38.3	36.49	4.7
Nayagarh	32.21	32.02	0.5
Nuapada	34.58	34.44	0.4
Puri	106.7	105.52	1.1
Rayagada	34.09	33.12	2.8
Sambalpur	55.63	54.22	2.5
Subarnapur	55.38	54.05	2.4
Sundargarh	59.33	57.28	3.4

Table 7. Temporal Changes in Estimated Cultivated and Irrigated Areas (2018-2023)

Year	Total Agriculture Area in rabi Season (thousand ha)	Irrigated Area in Rabi Season (thousand ha)
2018	2390.87	1869.26
2019	2370.21	1911.61
2020	2791.61	2343.39
2021	2465.12	2005.68
2022	2674.86	2203.53
2023	2722.17	2224.53

Mapping Irrigated areas in Odisha using Google Earth Engine (GEE)

by Aishwarya Vilas Desai
Adm No-221421311

Submission date: 20-Aug-2024 11:04AM (UTC+0530)
Submission ID: 2439570799
File name: plagarisum_chapter_I,_III,_IV,_V_1.docx (21.96M)
Word count: 7555
Character count: 45343

Mapping Irrigated areas in Odisha using GEE

ORIGINALITY REPORT

13%	11%	11%	6%
SIMILARITY INDEX	INTERNET SOURCES	PUBLICATIONS	STUDENT PAPERS

PRIMARY SOURCES

1	Ripudaman Singh. "Re-envisioning Remote Sensing Applications - Perspectives from Developing Countries", CRC Press, 2021 Publication	1%
2	www.mdpi.com Internet Source	1%
3	www.nfsm.gov.in Internet Source	1%
4	link.springer.com Internet Source	<1%
5	www.rkvy.nic.in Internet Source	<1%
6	courses.spatialthoughts.com Internet Source	<1%
7	Walter Timo de Vries, Iwan Rudiarto, N.M.P. Milinda Piyasena. "Geospatial Science for Smart Land Management - An Asian Context", CRC Press, 2023 Publication	<1%

8	www.int-arch-photogramm-remote-sens-spatial-inf-sci.net Internet Source	<1%
9	Submitted to Tata Institute of Social Sciences Student Paper	<1%
10	Submitted to University of Queensland Student Paper	<1%
11	er.nau.edu.ua Internet Source	<1%
12	Anwarelsadat Elmahal, Eltaib Ganwa. "Advanced Digital Image Analysis of Remotely Sensed Data using JavaScript API and Google Earth Engine", IntechOpen, 2024 Publication	<1%
13	Submitted to UNESCO-IHE Institute for Water Education Student Paper	<1%
14	www.researchgate.net Internet Source	<1%
15	Prasad S. Thenkabail. "Land Resources Monitoring, Modeling, and Mapping with Remote Sensing", CRC Press, 2015 Publication	<1%
16	oar.icrisat.org Internet Source	<1%

17	www.journaltocs.ac.uk Internet Source	<1 %
18	Submitted to Coventry University Student Paper	<1 %
19	C.H. Chen. "Image Processing for Remote Sensing", CRC Press, 2019 Publication	<1 %
20	www.researchsquare.com Internet Source	<1 %
21	www.sciencegate.app Internet Source	<1 %
22	Submitted to University of Arizona Student Paper	<1 %
23	Submitted to University of Witwatersrand Student Paper	<1 %
24	www.jorae.cn Internet Source	<1 %
25	"Climate Change Impacts on Natural Resources, Ecosystems and Agricultural Systems", Springer Science and Business Media LLC, 2023 Publication	<1 %
26	Richa Sharma, Surbhi. "Development of a Machine Learning Based Decision Support System for Rice Fungal Disease	<1 %

Management", 2023 6th International Conference on Contemporary Computing and Informatics (IC3I), 2023
Publication

27	Submitted to University of Melbourne Student Paper	<1 %
28	girs.ir Internet Source	<1 %
29	repository.unimilitar.edu.co Internet Source	<1 %
30	Aleksandra Wolanin, Gustau Camps-Valls, Luis Gómez-Chova, Gonzalo Mateo-García et al. "Estimating crop primary productivity with Sentinel-2 and Landsat 8 using machine learning methods trained with radiative transfer simulations", Remote Sensing of Environment, 2019 Publication	<1 %
31	Eli Yaswanth Kalyan, Raparthi Akshay, P. Selvi Rajendran. "Chapter 59 Machine Learning-Based Human Body Mass Index Prediction Using Facial Features", Springer Science and Business Media LLC, 2023 Publication	<1 %
32	Sunkara Naga Sindhu, Raavi Satya Prasad. "Dental Caries Detection Using Neural Turing Machines (NTM) and High Intensity Color	<1 %

	Detection (NTM-HICD) Model", Revue d'Intelligence Artificielle, 2024 Publication	
33	Submitted to University of Strathclyde Student Paper	<1 %
34	agritrop.cirad.fr Internet Source	<1 %
35	Submitted to Associatie K.U.Leuven Student Paper	<1 %
36	discovery.researcher.life Internet Source	<1 %
37	Submitted to Oklahoma State University Student Paper	<1 %
38	Ruchika Malhotra. "Empirical Research in Software Engineering - Concepts, Analysis, and Applications", Chapman and Hall/CRC, 2019 Publication	<1 %
39	Submitted to University of Southern Queensland Student Paper	<1 %
40	dokumen.pub Internet Source	<1 %
41	ses.library.usyd.edu.au Internet Source	<1 %

42	Edimilson Rodrigues dos Santos Junior. "Análise dos efeitos da mudança de cobertura da terra sobre a oferta de serviços ecossistêmicos em áreas úmidas periurbanas no estado de São Paulo", Universidade de Sao Paulo, Agencia USP de Gestao da Informacao Academica (AGUIA), 2023 Publication	<1 %
43	gcris2.iyte.edu.tr Internet Source	<1 %
44	"Cloud-Based Remote Sensing with Google Earth Engine", Springer Science and Business Media LLC, 2024 Publication	<1 %
45	Guangxing Wang, Qihao Weng. "Remote Sensing of Natural Resources", CRC Press, 2019 Publication	<1 %
46	Submitted to Middle East Technical University Student Paper	<1 %
47	Submitted to University of KwaZulu-Natal Student Paper	<1 %
48	eprints.whiterose.ac.uk Internet Source	<1 %
49	omu.repo.nii.ac.jp Internet Source	<1 %

50	ouci.dntb.gov.ua Internet Source	<1%
51	www.tandfonline.com Internet Source	<1%

Exclude quotes	On	Exclude matches	< 10 words
Exclude bibliography	On		

Aishwarya Vilas Dalai

PRJena
20.08.2024